Biochimica et Biophysica Acta 1783 (2008) 2061–2079

Contents lists available at ScienceDirect

Biochimica et Biophysica Acta

journal homepage: www.elsevier.com/locate/bbamcr

Review

Genome organization: Balancing stability and plasticity

Malte Wachsmuth [a], Maïwen Caudron-Herger [b], Karsten Rippe [b,*]

[a] European Molecular Biology Laboratory, Cell Biology and Biophysics Unit, Meyerhofstr. 1, 69117 Heidelberg, Germany
[b] Deutsches Krebsforschungszentrum and BioQuant, Research Group Genome Organization & Function, Im Neuenheimer Feld 280, 69120 Heidelberg, Germany

ARTICLE INFO

Article history:
Received 30 May 2008
Received in revised form 21 July 2008
Accepted 24 July 2008
Available online 3 August 2008

Keywords:
Genome organization
Nuclear structure
Fluorescence microscopy
Macromolecular dynamics and interactions
Diffusion

ABSTRACT

The cell needs to stably maintain its genome and protect it from uncontrolled modifications that would compromise its function. At the same time, the genome has to be a plastic structure that can dynamically (re) organize to allow the cell to adopt different functional states. These dynamics occur on the nanometer to micrometer length scale, i.e. ranging from the level of single proteins up to that of whole chromosomes, and on a microsecond to hour time scale. Here, we review different contributions to the dynamic features of the genome, describe how they are determined experimentally, and discuss the results of these measurements in terms of how the requirements for stability and plasticity are accommodated with specific activities in the nucleus.

1. The genome – organization and accessibility

1.1. Activities in the nucleus

The genomic DNA in eukaryotes is confined by the nuclear envelope to the cell nucleus. The genome-associated activities involve gene expression, DNA replication, recombination and repair, as well as RNA processing, mRNA transport and ribosome subunit assembly. Adopting a certain functional cell state requires a specific (re)organization of the genome to access the corresponding part of the DNA information while rendering other parts inactive. The degree of plasticity that can be achieved in the absence of changes of the DNA sequence information is remarkable when looking at the large variations of cell functions and morphology that are generated during development or in response to environmental factors. Furthermore, many fundamental changes of the cell state are reversible as for example demonstrated by the reprogramming of adult mouse and human somatic cells into "induced pluripotent stem cells" that appear to be functionally equivalent to native embryonic stem (ES) cells [1]. The selection of a certain cell program involves modifications of the chromatin state by post-translational modifications of histones and DNA [2–4], that often set marks to be read out by protein factors, as well as the activity of non-coding RNAs [5]. Moreover, the complex topological organization of the genome represents an additional control layer [6–9]. Together with the above-mentioned epigenetic factors it regulates the access to the DNA information. In addition, a number of nuclear activities are concentrated in subcompartments or organelles, which direct their localization to certain parts of the genome. These include the nuclear envelope [10,11], the nucleolus as the site of ribosome subunit biogenesis, transcription and replication factories [6,12], as well as Cajal [13] and PML (promyelocytic leukaemia) nuclear bodies (CB and PML-NB) [14] and SC35 domains ("speckles") [13,15], which represent mobile particles involved in RNA processing, transcriptional regulation and apoptosis.

1.2. Genome composition and nuclear environment

The genome of 2 × 3.2 billion bases (Gb) DNA in a human cell during the G1 phase of the cell cycle is organized in 24 chromosomes of 47 to 247 Mb in length and confined to the cell nucleus with typical diameters in the range of 10 to 20 μm. The same amount of free double-stranded DNA would occupy the volume of a sphere with a diameter of approximately 400 μm as estimated from its calculated radius of gyration. In the cell nucleus, the DNA is compacted by small highly positively charged proteins, the histones, into a large nucleoprotein complex designated as chromatin [16]. At the same time the genetic information has to remain accessible to DNA-binding factors involved in processes like replication, transcription, repair and recombination. Thus, the interaction of histones and DNA has to

Abbreviations: CB, Cajal body; PML, promyelocytic leukaemia; PML-NB, PML nuclear body; EJC, exon–exon junction complex; GFP, green fluorescent protein; NRL, nucleosome repeat length; MSD, mean squared displacement; SPT, single particle tracking; FRAP, fluorescence recovery after photobleaching; CP, continuous fluorescence photobleaching; FLIP, fluorescence loss in photobleaching; FCS, fluorescence correlation spectroscopy; FCCS, fluorescence cross-correlation spectroscopy; FRET, fluorescence resonance energy transfer; ICS, image correlation spectroscopy; ET, energy transfer; ROI, region of interest; NLS, nuclear localization signal; SMC, structural maintenance of chromosomes; HP1, heterochromatin protein 1; ES cells, embryonic stem cells; TFIIH, transcription factor II H

* Corresponding author. Tel.: +49 6221 54 51376; fax: +49 6221 54 51487.
E-mail address: karsten.rippe@bioquant.uni-heidelberg.de (K. Rippe).

0167-4889/$ – see front matter © 2008 Elsevier B.V. All rights reserved.
doi:10.1016/j.bbamcr.2008.07.022

mediate between these two functions in a dynamic manner. The basic building block of chromatin is the nucleosome, which consists of 146/147 base pairs (bp) wrapped around a histone octamer protein core. The nucleosome repeat length (NRL) varies between 165 and 220 bp of DNA depending on the species and also on the cell type within a given organism and amounting to about 200 bp in mammals [16]. Accordingly, 6.4 Gb or 7 pg DNA in a human cell are assembled into ~30 million nucleosomes. At physiological salt concentrations, the chain of nucleosomes on the DNA can reversibly fold into a fiber with a diameter of approximately 30 nm (Figs. 1 and 2, [16–19]). For native fiber fragments, a linear mass density of 6–7 nucleosomes per 11 nm fiber has been reported [20,21]. In the following, it is assumed that the chromatin fiber conformation persists during interphase in the nucleus. However, it is noted that the ultrastructural identification of the folding of the nucleosome chains into a fiber as well as its higher order organization in the cell remains a challenge even with current state-of-the-art electron microscopy approaches (see for example [22–24]). Some evidence for the formation of alternative more globular nucleosome aggregates has been reported as discussed in ref. [16].

Chromatin contains histone proteins and DNA at a concentration of 7 mg ml^{-1} and 19 mg ml^{-1}, respectively, occupying ~10% of the total nuclear volume when assuming its compaction into a 30 nm chromatin fiber. Protein concentrations of 110 mg ml^{-1} in the nucleoplasm and 140–220 mg ml^{-1} for nuclear subcompartments like nucleoli, CB and speckles/SC35 domains [25] have been measured, while ion concentrations amount to ~0.1 M of K^+/Na^+ ($[K^+]>[Na^+]$), 0.5–1 mM of Mg^{2+} and low μM values of Ca^{2+} [25,26]. The average RNA concentration in the nucleus is 11–15 mg ml^{-1} (reviewed in ref. [27]) leading to a nucleic acid concentration of 30–35 mg ml^{-1}. Accordingly, the total concentration of macromolecules in the nucleus adds up to ~200 mg ml^{-1} occupying 20–30% of the nuclear volume. Thus, the DNA genome is embedded in a viscous liquid that is densely packed with macromolecules. On the one hand, this environment promotes macromolecular interactions and the formation of subcompartments due to molecular crowding as discussed elsewhere in this issue [28]. On the other hand, it imposes a number of constraints with respect to the mobility of factors and the accessibility of nuclear space that need to be considered in a description of macromolecular interactions in the nucleus.

1.3. Genome organization and DNA accessibility

1.3.1. Nucleosomes

On the molecular level, access to the DNA is regulated by the nucleosome positions. The wrapping of DNA around the histone octamer complex has long been recognized as a mechanism to inhibit access to this part of the DNA sequence as compared to the linker DNA region. The nucleosome represents a relatively stable structure and studies on its *in vitro* stability have been reviewed elsewhere [29]. Changes of nucleosome positions at promoter and enhancer regions can directly affect gene regulation [30–33]. The nucleosome positions are determined by three major contributions: (i) The intrinsic binding affinity of the histone octamer depends on the DNA sequence, and a number of natural and artificial high-affinity binding sequences have been identified [34]. Furthermore, a growing data set has correlated *in vivo* nucleosome positions with their affinities to different DNA sequences [35–37]. (ii) The nucleosome can be displaced or recruited by the competitive or cooperative binding of other protein factors [38]. (iii) The nucleosome may be actively translocated or evicted by ATP-dependent remodeling complexes [31,39–41]. Moreover, recent experiments have shown that the remodeling reactions are directed also by the DNA sequence and that different nucleosome remodeling complexes display characteristic translocation activities in this respect [42].

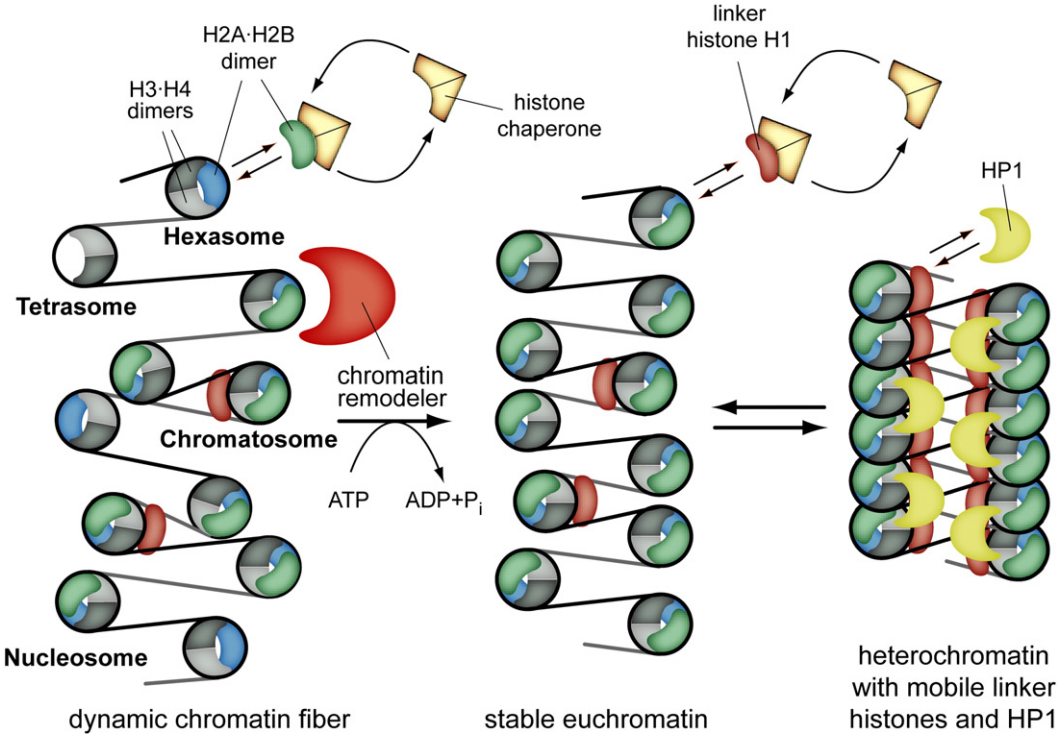

Fig. 1. Chromatin dynamics: Histones and other protein factors that control the chromatin state. The model is derived from an analysis of nucleosome assembly [160]. It is postulated that in a nascent dynamic chromatin state the interaction of histone chaperones with (sub)nucleosomal particles results in formation of an unordered chromatin chain that contains hexasomes, nucleosomes and chromatosomes with an irregular spacing on the DNA and constant exchange of histones. This chain is converted into a regular structure by ATP-dependent remodeling machines that induce a regular spacing of nucleosomes. In this conformation a chromatin fiber is established, in which the nucleosomes are stabilized and histone dissociation is inhibited. In contrast, the histone chaperone-mediated binding and dissociation of linker histone is still possible [159]. Targeted by epigenetic signals, chromosomal proteins like HP1 bind to the chromatin fiber and stabilize a specific chromatin state [234].

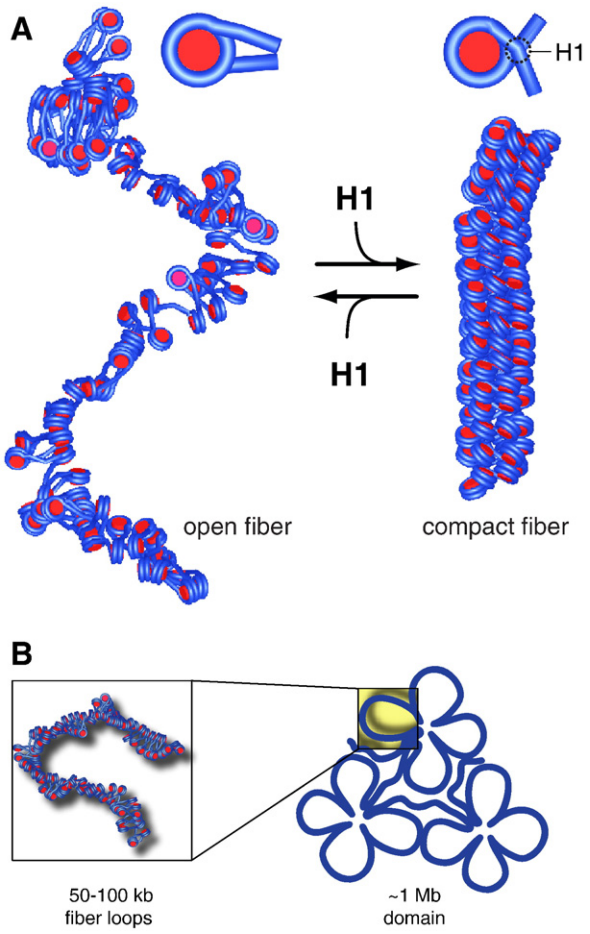

Fig. 2. Chromatin dynamics: Chromatin fiber and higher order folding. (A) Model for chromatin fiber compaction induced by binding of linker histone H1. The left fiber represents an open conformation with straight linker DNA in the absence of linker histones, in which DNA access is facilitated for other proteins. The binding of linker histone H1 changes the local nucleosome geometry. This induces a transition to more compacted fiber conformations in which the DNA is less accessible [49,50]. (B) Hypothetical model for the higher order folding of the 30 nm chromatin fiber during interphase leading to the formation of 1 Mb chromatin domains. A rosette like structure according to the radial-loop model is shown [54–57]. However, alternative structures such as the random-walk/giant loop [58] or the chromonema model [59–61] have also been proposed.

1.3.2. Chromatin fibers

While the structure of the nucleosome is known at atomic resolution [43], the structure of the 30 nm fiber remains controversial, and various models for the fiber geometry are currently under investigation [16–19]. The available experimental data support the existence of at least three main types of different fiber conformations, which are distinct with respect to the presence or absence of linker histones, the source of nucleosomes and the NRL: (i) A two-start fiber helix that can be derived from the crystal structure of a tetranucleosome particle [44]. This structure has a short NRL of 169 bp and was determined in the absence of linker histones. (ii) A one-start helix with interdigitated nucleosomes that is based on electron microscopy studies of chromatin fibers reconstituted *in vitro* with NRLs of 177–237 bp and one linker histone per nucleosome [45,46]. (iii) A two-start helix conformation with crossed-linker DNA as proposed on the basis of electron microscopy studies of native chromatin fibers extracted from chicken erythrocytes. These showed a zig-zag-like DNA backbone with a so-called nucleosome stem motif induced by the binding of linker histone H1/H5 [47,48]. The stability of these three different types has been evaluated recently in Monte Carlo simulations of nucleosome chains with different local geometries and NRLs [49,50].

The folding of the nucleosome chain can restrict the access to the linker DNA significantly, and a 50-fold difference has been reported based on a comparison of dinucleosomes with 17mer nucleosome arrays [51]. In addition, the binding of linker histone H1 induces a compaction of the fiber structure [19,45]. A model for this transition is shown in Fig. 2A in which H1 compacts a fiber with zig-zag shape and straight accessible linker DNA into a compact structure that has most of the linker DNA in its interior so that access to it is impeded [19,49].

1.3.3. Higher order folding of the chromatin fiber

Several lines of evidence indicate that the chromatin fiber adopts a higher order folding that organizes the interphase chromosome into domains containing roughly 1 Mbp of DNA [52]. Using high resolution light microscopy, an apparent bead-like structure of chromatin can be observed, in which chromatin domains of this size are more densely packed into an approximately spherical substructure of 300–400 nm diameter [53]. However, the spatial and temporal resolution of the light microscope is not sufficient to identify the organization of the 30 nm chromatin fiber that leads to the formation of the ~1 Mb domains. Different conformational states have been proposed: in the radial-loop model, the 30 nm fiber forms loops of roughly 100 kb size that are arranged into rosettes [54–57] (Fig. 2B). The random-walk/giant-loop model suggests the looping of large regions of chromatin (3 Mb) and their tethering to a backbone-like structure [58]. In the chromonema model [59–61], the compaction of the 30 nm fiber is achieved by its folding into 60–80 nm-sized structures that undergo additional folding into so-called chromonema fibers of 100–130 nm in diameter.

1.3.4. Chromosome organization

During interphase the confinement of individual chromosomes to certain regions of the nucleus referred to as “chromosome territories” has been demonstrated using whole chromosome painting probes and fluorescence *in situ* hybridization (FISH) [62–64]. This aspect of genome organization is elucidated in detail in a number of reviews [52,65,66]. Chromosome territories have an irregular shape and occupy discrete nuclear positions with little overlap or intermingling, the extent of which is currently under investigation [7,66,67]. The territorial organization of chromosomes persists stably even in post-mitotic cells [52,65]. Intrachromosomal linkages are likely to be involved in establishing and maintaining chromosome territories via a net-like organization of the chromatin fiber during interphase [66,68,69]. The relative location of genome loci within a chromosome territory and with respect to the complete nucleus has been related to transcriptional activity [6–9,52,65,66]. In general, gene-rich chromosomes appear to be located preferentially in the nuclear interior and gene-poor chromosomes more at the nuclear periphery. In agreement with this, non-transcribed sequences were found more frequently at the nuclear periphery or in perinucleolar areas, which are regions of high chromatin density (see below). These are referred to as heterochromatin as opposed to the less dense euchromatin, and are characterized by an enrichment of repression histone methylation marks and the binding of heterochromatin protein 1 (HP1) [16,70,71]. Interestingly, specific chromosomal regions at the nuclear periphery make direct contacts with the nuclear lamina [6,10,11]. These sites have been mapped recently with high resolution in human fibroblasts, showing that the lamin B1-interacting chromatin domains are indeed associated with low gene expression and a repressive chromatin conformation [72]. Active genes and gene-rich regions tend to localize on chromosome surfaces exposed to the nuclear interior or on loops extending from the territories [8].

During mitosis chromosomes experience an additional level of compaction. Current models for the folding of chromatin into mitotic chromosomes can be found in recent reviews [73,74]. Establishing the mitotic chromosome structure requires the condensin I and II complexes that contain the structural maintenance of chromosomes

(SMC) proteins [75]. These induce the folding of metaphase chromosomes. During this process, the SMC2 protein progressively accumulates in the central chromatid axis serving as a self-organizing inner "glue" to mediate the hierarchical folding of a chromosome into its fully condensed state [75,76].

1.4. Accessibility of nuclear space

Assuming an average spacing of the chromatin fiber, some estimates on the accessibility of this fiber network can be made on the basis of nucleosome and/or DNA concentration measurements and experimental studies on the distribution of particles with different sizes in the nucleus (Table 1, Fig. 3). An average nucleosome concentration of 0.14 mM [77] or the equivalent of 18–19 mg ml^{-1} DNA ([27] and references therein) have been reported for mammalian cell lines. This yields a nuclear volume of 0.4 pl , which is in agreement with direct size measurements. A bulk of the more densely packed heterochromatin has nucleosome concentrations of 0.2–0.3 mM with a small heterochromatin fraction (~10%) reaching a nucleosome density of 0.4–0.5 mM as inferred from fluorescence microscopy-based measurements [77,78] (Fig. 3). It is noted that an only moderate two-fold difference in terms of the density observed for euchromatin and bulk heterochromatin does not exclude higher compaction differences on a smaller length scale that are not resolved by optical methods. In a recent study, a characteristic tightly packed chromatin ultrastructure was revealed for the inactive X chromosome that was not apparent from a light microscopic comparison of the volume occupied by the inactive and active X chromosome [24]. Other heterochromatin domains visible on fluorescence microscopy images have dimensions in the micrometer scale and are mostly found at the nuclear periphery, around the nucleolus and at the centromeres. Their compaction state and accessibility is affected by histone modifications like acetylation [78,79] and a decondensation occurs upon the induction of transcription [80].

During interphase, particles up to ~20 nm in size experience no restrictions with respect to their nuclear distribution within the 200–300 nm resolution limit of light microscopy [78,81,82] (Table 1). Particles with a size of ≥30 nm like 150 kDa and larger FITC-labeled dextrans are progressively excluded from dense chromatin regions. Particles with sizes around 100 nm (100 nm diameter nanospheres, 2.5 MDa dextrans) are completely excluded from the chromatin mesh [83,84]. This is also relevant for CBs and PML-NBs with sizes of 0.1–1 μm, which therefore have access to a subspace of the nucleus only. Fast translocations of these bodies are confined to distances of only a few hundred nanometers in regions that are at least transiently devoid of chromatin [85]. Above this length scale a greater chromatin reorganization is required that allows the separation of chromatin subdomains in order to create accessible regions within and through the chromatin network. The interface between chromosome territories can be visualized via the polymerization of nuclear localization signal (NLS)-containing vimentin filaments that form between chromosome territories and display a co-localization with nuclear bodies [86–90] or by inducing chromatin condensation [67,91]. Changes of the compaction state induced via factors like histone acetylation, ATP depletion or by osmolarity variations of the medium appear to occur in a reversible manner as discussed previously [69].

In the mitotic chromosome, chromatin is further compacted and a concentration of 1.2–1.3 mM nucleosomes and 170 mg ml^{-1} DNA is reached, which is ~10-fold higher than the average chromatin density during interphase [92]. This corresponds to the local nucleosome concentration in a closely packed 30 nm chromatin fiber with 6–7 nucleosomes per 11 nm fiber. It has been proposed that such a high nucleosome concentration could induce the resolution of a distinct 30 nm fiber into a more homogenous liquid phase-like aggregate of nucleosomes devoid of periodic structure [73,93]. In terms of accessibility, proteins up to the dimensions and molecular weight of that of a nucleosome (11 nm diameter, ~200 kDa) can access the chromatin fiber network even in its most compacted state during metaphase, while dextrans with an ~18 nm diameter are excluded [78,94].

Table 1
Nuclear diffusion coefficient and accessibility of inert particles

Particle	*M* [kDa]	Size [nm]	*D* [$\mu m^2 s^{-1}$]	Accessibility	References
GFP	30	4[a]	23±4	Unrestricted	[82,111,121]
GFP_2	60	8[b]	15±1	Unrestricted	[82]
GFP_3	90	12[b]	12±1	Unrestricted	[82]
GFP_4	120	16[b]	9±1	Unrestricted	[82]
GFP_5	150	20[b]	8±1	Unrestricted	[82]
Dextran	4	7[c]	23±2	Unrestricted	[78,235]
Dextran	150	25[c]	6±1	Mostly unrestricted	[78,235]
Dextran	500	46[c]	4±2	Partially excluded	[78,235]
Dextran	2500	110[c]	n. d.	Excluded	[78]
nanospheres	n.d.	100	$4{\cdot}10^{-4}$	Excluded	[84]
Mx1-YFP	n.d.	1300	$1.8{\cdot}10^{-4}$	Excluded	[85]

M is the molecular weight and *D* is the diffusion coefficient.
[a] GFP is a cylinder with ~3 nm diameter and ~4 nm height [236]. In water at 25 °C diffusion coefficients of 87 $\mu m^2 s^{-1}$ [237] and 76 $\mu m^2 s^{-1}$ [82] were reported for a GFP monomer yielding an average value of 81 $\mu m^2 s^{-1}$.
[b] The monomer dimensions (4.1 nm diameter sphere) were used as the dimension of the repeating unit for the GFP multimers to determine the extensions along the long axis.
[c] The size is given as two times the radius of gyration of the dextran random coil polymer.

2. Theoretical framework for describing macromolecular dynamics

2.1. General considerations

The different levels of genome organization as described above correspond to, require, and result in dynamic processes on various scales: (i) The core protein components of chromatin bind to and dissociate from the DNA. These include core and linker histones as well as other chromosomal proteins like HP1 (Fig. 1). (ii) The nucleosome binding position on the DNA can be modulated by ATP-hydrolyzing remodeling complexes that can also evict nucleosomes. (iii) Genomic loci themselves are mobile within the nucleus. (iv) The various supramolecular complexes and nuclear subcompartments that harbor certain chromatin-modifying activities feature a dynamic composition and experience a continuous turnover of their components. Furthermore, they can translocate within the chromatin network. In order to characterize these dynamics on different time and length scales various fluorescence microscopy-based methods like FRAP (fluorescence recovery after photobleaching), SPT (single particle tracking) or FCS (fluorescence correlation spectroscopy) have been developed.

A fundamental contribution to the mobility of macromolecules in the nucleus is diffusion or Brownian motion, i.e. thermally induced random movement. Diffusion attempts to balance macroscopic concentration gradients, for example created by active transport or generated by depleting the fluorescence from a certain area of a cell (experimentally exploited with FRAP as described below). The diffusion coefficient characterizes the relation between the gradient and the resulting flux. On a microscopic scale, single molecules roam randomly through their environment, thus generating distinct local concentration fluctuations (experimentally exploited with FCS, see below). The area covered by roaming or the mean squared displacement (MSD), respectively, go linear in time, the proportionality factor being the diffusion coefficient, which is usually given in square micrometers per second ($\mu m^2 s^{-1}$).

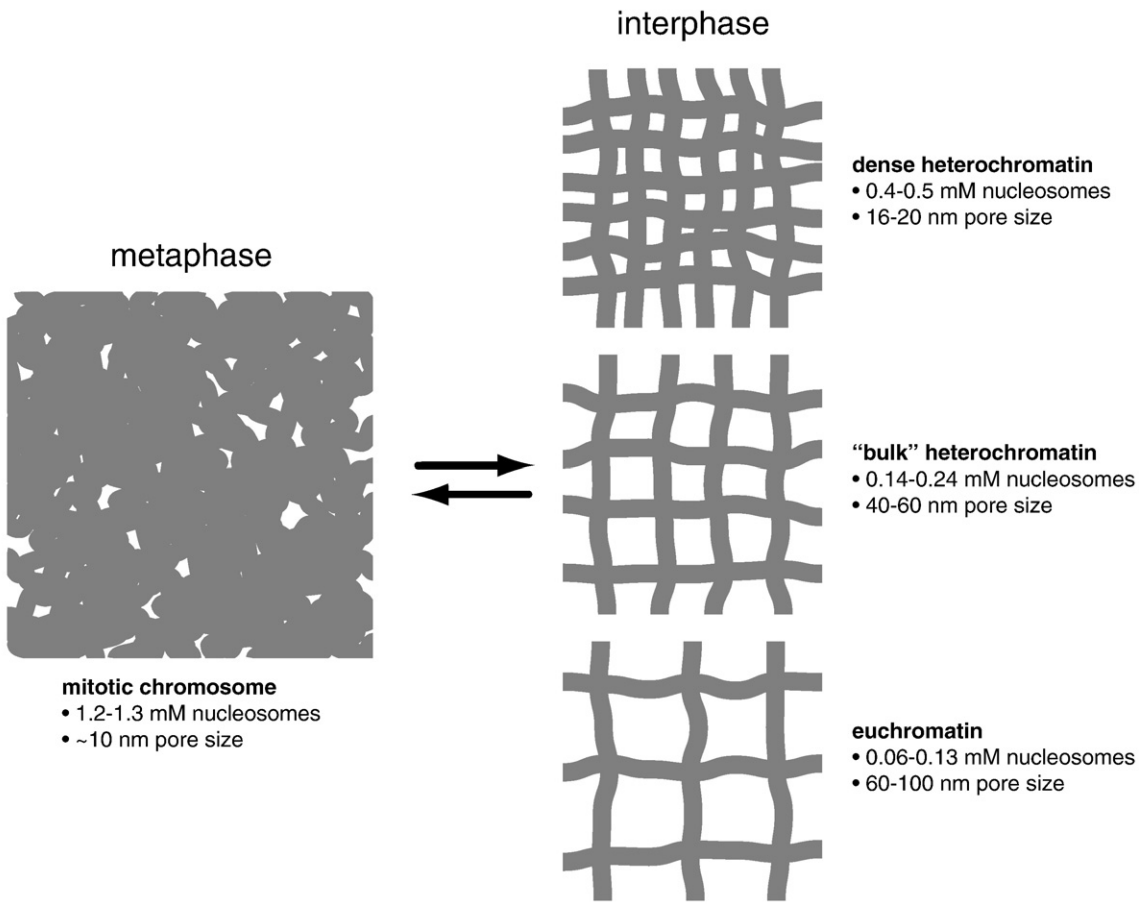

Fig. 3. Accessibility of nuclear space. Different chromatin condensation states as determined from density and accessibility measurements (see text and Table 1). Average pore sizes represent a particle size limit that can still access a given compaction state.

Various processes can affect the diffusive behavior (Fig. 4): (i) Molecules are slowed down when associating into larger yet mobile complexes. The actual diffusion coefficient is reduced. (ii) The diffusion can deviate significantly from free diffusion, i.e. the MSD goes less than linear in time, in complex environments like the cell nucleus or heterogeneous membrane systems, resulting in anomalous,

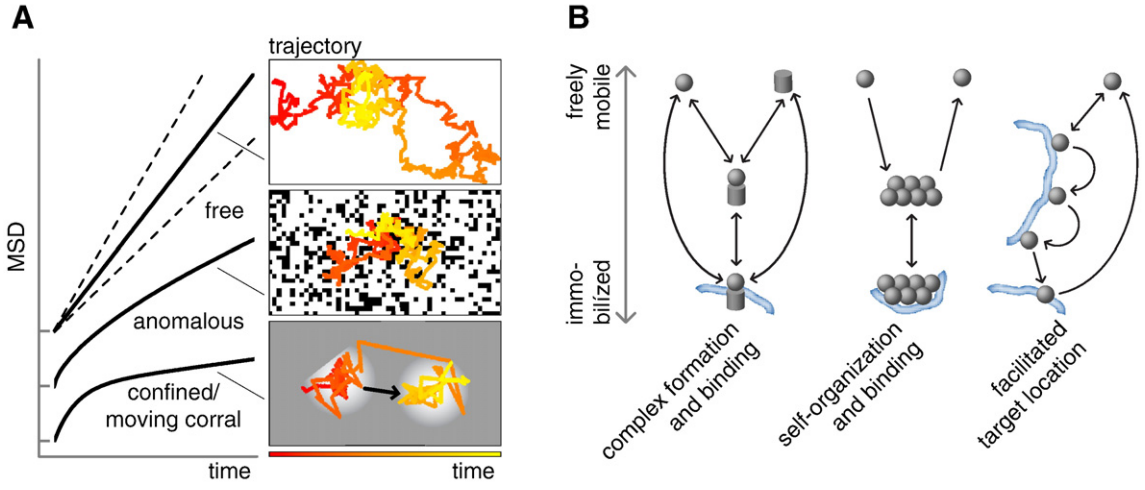

Fig. 4. Diffusion modes and mobilities. (A) Different modes of diffusion each represented by the MSD and exemplary trajectories. These are based on simulated and measured [85] random walks on a two-dimensional rectangular lattice (time progress is symbolized by color transition from red to yellow). Top: Free diffusion with a MSD linear in time. A higher diffusion coefficient results in a steeper slope and vice versa. Middle: Anomalous diffusion occurs in the presence of (randomly organized) obstacles where the MSD goes less than linear in time and the area covered becomes more compact. Bottom: In the case of the confined diffusion/moving corral model, the MSD shows a biphasic behavior: for short times, the fast random motion of a particle is restricted to the highlighted confinement area and the MSD approaches rapidly an apparently constant value. For longer times, the confinement area itself diffuses slowly, resulting in a slow linear increase of the MSD. (B) Different models for the binding of molecules and complexes to specific binding sites and their impact on molecular mobilities: the factors involved can be found as highly mobile free fractions, as fractions of reduced mobility due to the integration into larger complexes and self-organized multimers or due to hopping- or sliding-like facilitated diffusion, and as fractions bound to (apparently) immobilized structures like chromatin.

obstructed or confined Brownian motion [95]. (iii) Specific binding of molecules to cellular structures results in immobilization and leads to a reduced effective mobility.

It is useful to specify two limiting cases [96–99]. In the presence of a substantial free fraction of molecules, these redistribute rapidly, most of the binding sites are occupied, and the corresponding kinetics are dominated by the dissociation process. The binding can be approximated as a first-order reaction and a free and a bound fraction can be distinguished. The other case is the regime of limited diffusion where a sufficient number of binding sites are not occupied. When a molecule is released, it is rapidly recaptured by another site and the molecules appear as one fraction with a reduced effective diffusion coefficient.

While Brownian motion is a very energy-efficient mode of transport the occupation of sparsely distributed target binding sites with the correct factors or complexes can still be a rare event. However, formation of the specific complex can be accelerated by nonspecific interactions that can increase the association rates well beyond the diffusion limit (Fig. 4B) [100–103].

2.2. Free translational diffusion

The translational diffusion of a free particle is a thermally induced random movement resulting from continuous collisions with solvent molecules, which convey kinetic energy of $m\langle v_x^2\rangle/2 = k_B T/2$ per dimension x to a particle of velocity v and mass m at temperature T where k_B is the Boltzmann constant and $\langle\ldots\rangle$ denotes time/ensemble averaging. Owing to the random nature of diffusion, both mean velocity and displacement are zero and the MSD $\langle d^2\rangle$ is used to characterize the motion (Fig. 4A). It is defined as the square distance of the positions $\vec{r}(t)$, $\vec{r}(t+\tau)$ the particle occupies before and after time intervals of length τ, averaged over all available steps of a trajectory and all particles:

$$\langle d^2(\tau)\rangle = \left\langle [\vec{r}\,(t+\tau)-\vec{r}(t)]^2 \right\rangle = 2nD_0\tau. \quad (1)$$

Here, n is the dimensionality of the system and D_0 the diffusion coefficient, both defining the slope of the MSD versus time. Macroscopically, the diffusion coefficient quantifies the relation between a concentration gradient and the resulting flux. Microscopically, it depends on the absolute temperature T and the friction coefficient f according to the Stokes–Einstein relation:

$$D_0 = \frac{k_B T}{f}. \quad (2)$$

The radius of a sphere with the same friction coefficient defines the hydrodynamic radius R_h of a macromolecule. Following Stokes' law and inserting the solvent viscosity η shows that the diffusion coefficient is reversely proportional to the effective size of the molecule:

$$D_0 = \frac{k_B T}{6\pi\eta R_h}. \quad (3)$$

The shape of the molecule or complex determines how D_0 depends on the molecular weight M according to $R_h \propto M^d$ with $d \sim 1/3$ for globular molecules or $d \sim 1/2$ for polymers.

2.3. Anomalous diffusion

In more complex environments containing statistically organized obstacles like fixed structures or larger particles of lower mobility we have to consider deviations from simple random-walk behavior resulting in obstructed diffusion [104]. Phenomenologically, it can be described by means of the concept of anomalous diffusion (Fig. 4A) where the MSD does not follow linear time dependence but rather obeys:

$$\langle d^2(\tau)\rangle = 2n\Gamma\tau^\alpha = 2nD(\tau)\tau \quad \text{with} \quad D(\tau) = \Gamma\tau^{\alpha-1} \quad (4)$$

The anomaly parameter α quantifies the deviation from free diffusion, which is obtained for $\alpha = 1$. In the case of obstructed diffusion, $\alpha < 1$, and in the case of ballistic or directed movement, $\alpha > 1$ is observed. As a constant diffusion coefficient cannot be defined, the MSD is characterized by a transport coefficient Γ or a time-dependent diffusion coefficient $D(\tau)$ [105–107].

Collisions with obstacles result in a deviation from free diffusion in space and thus in anomalous diffusion. In addition, nonspecific binding to randomly distributed sites showing a broad distribution of binding energies with a width of ε can occur. This can be described with the continuous time random-walk model [108,109]. When ε is larger than $k_B T$, an increased deviation from free diffusion in time sets in and the anomaly parameter is further reduced to

$$\alpha' = \alpha\frac{k_B T}{\varepsilon}. \quad (5)$$

2.4. Confined diffusion

If the MSD data deviate systematically from a linear (Eq. (1)) or simple power law time dependence (Eq. (4)), more complex models must be applied for a quantitative description of the particle mobility. For example, when a particle with a free diffusion coefficient D_{fast} is confined to a "corral" with radius r_c (more precisely its radius of gyration), the MSD can be approximated with Eq. (2) in the short time limit and is stationary at $\langle r_c^2\rangle$ in the long time limit [85,95,110] leading to:

$$\langle d^2(\tau)\rangle = \langle r_c^2\rangle\left[1-\exp\left(-\frac{2nD_{fast}\tau}{\langle r_c^2\rangle}\right)\right]. \quad (6)$$

An additional contribution due to a more global mobility of the confined loci can be described in a so-called "moving corral" model according to Eq. (7) (Fig. 4A). Here, the overall mobility is determined by three parameters: the particle experiences fast but confined diffusion with a coefficient D_{fast} in a corral with radius r_c. These corrals can also translocate according to a free diffusion model with a diffusion coefficient D_{slow}:

$$\langle d^2(\tau)\rangle = \langle r_c^2\rangle\left(1+\frac{2nD_{slow}\tau}{\langle r_c^2\rangle}\right)\left[1-\exp\left(-\frac{2nD_{fast}\tau}{\langle r_c^2\rangle}\right)\right] \quad (7)$$

In case the corrals do not translocate, i.e. for $D_{slow} = 0$, one obtains Eq. (6) [85].

2.5. Reaction–diffusion processes

As mentioned above, the molecules of interest are often present in several interacting and exchanging fractions differing in mobility and binding state, e.g. fully immobilized and freely mobile fractions as well as larger yet diffusive complexes (Fig. 4B). For a comprehensive description of their spatio-temporal behavior, one has to extend the differential equation for the concentration or probability distribution $c_m(\vec{r},t)$ in the case of pure diffusion of a single species m

$$\frac{\partial c_m(\vec{r},t)}{\partial t} = D_{0,m}\vec{\nabla}^2 c_m(\vec{r},t) \quad (8)$$

from which Eq. (1) can be obtained. This leads to a set of coupled differential equations for M species including both reaction and diffusion terms [111]:

$$\frac{\partial c_m(\vec{r},t)}{\partial t} = D_{0,m}\vec{\nabla}^2 c_m(\vec{r},t) + \sum_{n\neq m}\left[k_{nm}c_n(\vec{r},t) - k_{mn}c_m(\vec{r},t)\right] - k_{-,m}c_m(\vec{r},t) + k_{+,m} \quad \text{for } m = 1,\ldots,M \tag{9}$$

Here, $D_{0,m}$ is the diffusion coefficient of species or fraction m and $\vec{\nabla}^2$ the Laplace operator. The rate constants k_{mn} represent transformation processes between the fractions due to association/dissociation whereas $k_{-,m}$ and $k_{+,m}$ stand for the creation and destruction of fraction m independent of the others. It should be noted that the rate constants themselves can vary in time and space, too. For instance, photobleaching can be covered by $k_{-,m} = k_{-,m}(\vec{r},t)$. A solution of such a system must take into account the nuclear or cellular topology and the initial concentrations as boundary conditions. It must be transformed into observables as provided by the methods used, e.g. the intensity integrated over a region or intensity fluctuations in a small volume or the trajectory of a particle. Subsequently a fit to the experimental data is conducted in order to obtain physical parameters like diffusion coefficients or association and dissociation rates.

2.6. Facilitated diffusion

For many biological functions in the nucleus, it is crucial that proteins and complexes locate their specific binding sites on chromatin and DNA. However, especially for sparsely distributed sites, a diffusion-controlled roaming is far too slow and the expected association rates do not match the experimental observations, as it was first observed for *Escherichia coli* LacI repressor binding to λ DNA (for review see [100]). Hence, the model of facilitated diffusion was introduced suggesting that collisions of the protein with DNA are inelastic due to nonspecific interactions (Fig. 4B). This enables the protein to slide along the DNA (effective one-dimensional diffusion), to hop along the strand (a fast sequence of dissociation and reassociation), or to jump from one segment to another (either on the same or on different molecules, facilitated by random or sequence-dependent looping). Assuming sliding as the dominant process [101,112], the diffusion-limited association rate per protein molecule k_0 is approximately increased to:

$$k = k_0\left(\frac{a}{l_{sl}} + \frac{D_0}{D_{sl}}\frac{l_{sl}}{a}a^2 L l_{sl} c\right)^{-1} \tag{10}$$

Here, a is the reaction distance, i.e. the distance between protein and target size required for actual binding, l_{sl} the average sliding length, D_0 the solvent diffusion coefficient and D_{sl} the sliding diffusion coefficient. L stands for the DNA contour length and c for the DNA concentration in molecules per volume element. Under realistic conditions, this can result in an increase of up to two orders of magnitude. This is apparent from comparing the search time τ of a particle to find its target in one, two or three dimensions [102]. While τ scales with R^3 for searching a spherical volume with radius R, it is proportional to R^2 in one dimension and R^2 times a usually small logarithmic factor in two dimensions.

3. Measuring dynamics and interactions of nuclear components

3.1. Time scales and resolution

The mobility of proteins, nucleic acids, complexes or nuclear bodies inside nuclei of living cells can be studied using a number of fluorescence microscopy-based techniques (Fig. 5). FRAP is the most prominent member of a whole family of methods such as continuous photobleaching (CP) or fluorescence loss in photobleaching (FLIP) [113,114]. These methods are all based on photoinduced bleaching (or activation) of marker molecules in selected areas of a cell and subsequent or simultaneous relaxation back to equilibrium. FCS stands for a complementary set of related methods employing thermal equilibrium fluctuations in order to determine diffusion properties and interactions [115–117]. For larger particles that can be identified in the light microscope, the mobility can be analyzed by single particle tracking methods (SPT), in which a time series of images is collected to determine the movement of the particle over time [118]. In a somewhat different approach not based on mobilities, the interaction of molecules can be detected with fluorescence resonance energy transfer (FRET) [119,120], an effect serving as "proximity sensor" for appropriately labeled molecules of interest. All these techniques are now widely used since they can be routinely implemented on commercial confocal or widefield fluorescence microscopes.

Typical applications from studies on nuclear structure and dynamics range from the characterization of protein and RNA diffusion by FCS [121,122] or of binding properties of chromatin proteins by FRAP [123–125] via tracking of single proteins [126], large nuclear bodies [85] or chromatin loci [127] to the identification of spliceosome assembly steps by FRET [128]. These processes occur on different time scales between microseconds and hours (Fig. 6A) not least because the local accessibilities and mobilities are size-dependent and frequently reflect features of the chromatin environment. Correspondingly, different methods cover different yet overlapping time regimes (FCS: 1 μs – 1 s; FRAP: >100 μs; SPT: >10 ms; Fig. 6A) while they can be all be used (in principle) with diffraction-limited spatial resolution. Thus, they provide complementary information so that they can be chosen and combined appropriately (Fig. 6B).

3.2. Single particle tracking

As depicted in Fig. 5, an SPT study of intracellular particles or structures requires (i) the acquisition of a time series of fluorescence images or image stacks; (ii) correction for any movements of the whole cell (as described in [129,130]); (iii) segmentation of the images in order to identify the particles of interest; (iv) extraction of a trajectory, i.e. a time series of position coordinates, for each particle. From these raw data, the MSD can be computed as described above (Eq. (1)). By fitting an appropriate model function, which represents the underlying biophysical process of movement, parameters like a diffusion coefficient or a confinement radius can be derived as discussed above. The mean displacement $\langle\vec{r}(t+\tau)-\vec{r}(t)\rangle$ allows it to identify remaining non-random movements or to determine short range velocities (defined as displacement per time interval). A simple way to remove non-random translational and rotational movements for example of the whole cell is the calculation of mean square distance changes and the mean square displacement of the center of mass, respectively.

Since SPT provides the MSD as an immediate readout, the identification of different diffusional modes is straightforward. A plot of the MSD versus time allows to distinguish free diffusion, anomalous or obstructed diffusion, confined diffusion and directed motion (Fig. 4A). In a fit of the MSD versus time relationship experimental values of $\alpha<1$ may be considered as characteristic for confined diffusion, $0.9<\alpha<1.1$ indicative of free diffusion, $0.1<\alpha<0.9$ are interpreted as obstructed diffusion, while $\alpha>1.1$ represents directed motion. It should be noted that due to random variations even in the case of free diffusion a value close to $\alpha\approx 1$ will only be obtained if a sufficiently high number of data points is averaged. For the movement of a freely diffusing particle, time periods can be selected from a single trajectory, in which the particle moves with an apparent higher or lower α. In order to distinguish these variations from the existence of distinct classes of particles, a histogram of the values of α or other parameters derived from SPT can be a useful diagnostic tool.

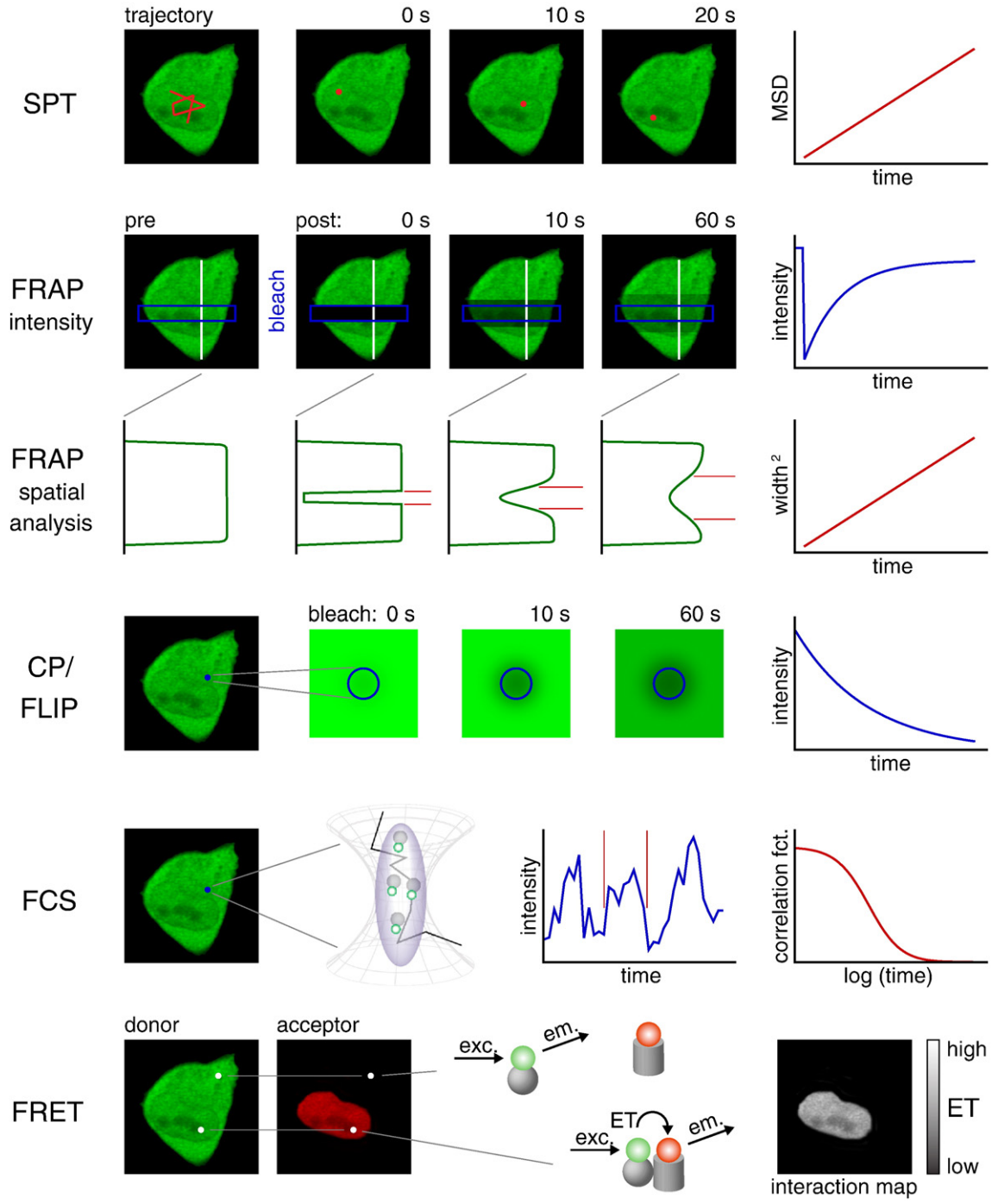

Fig. 5. Fluorescence microscopy methods to analyze the dynamic genome organization in living cells. A summary of different complementary fluorescence microscopy-based methods is depicted schematically. *SPT (single particle tracking)*: positions of a single particle at different time points in a cell (red), the resulting trajectory and the MSD. *FRAP (fluorescence recovery after photobleaching) intensity measurements*: a cell with a bleach region (ROI, blue) and a line for profile analysis (white) at different pre- and postbleach time points and the averaged intensity in the ROI plotted versus time. *FRAP spatial analysis*: intensity profile along the white line at different pre- and postbleach time points and the squared width of the bleached strip plotted versus time. *CP/FLIP (continuous photobleaching/fluorescence loss in photobleaching)*: a cell with a bleach spot (blue), a magnified view at different time points, and the spot intensity plotted versus time. *FCS (fluorescence correlation spectroscopy)*: a cell with a measurement spot (blue), a magnified view of the focus, the time course of intensity fluctuations and the intensity autocorrelation function. *FRET (fluorescence resonance energy transfer)*: a cell with the fluorescence signal in the donor and the acceptor channel with two reference spots (white) with and without energy transfer (ET) between donor and acceptor fluorophores, the concept of FRET as a function of molecular proximity/interaction with donor excitation (exc.) and donor or acceptor emission (em.) and the resulting interaction map with ET as signal.

3.3. Fluorescence recovery after photobleaching

A typical imaging-based FRAP experiment in a living cell consists of (at least) three steps (Fig. 5): (i) a time series of prebleach images of the cell in order to record the *bona fide* equilibrium distribution of the fluorescently labelled molecules of interest; (ii) the bleach sequence, in which the region of interest (ROI) of the cell is depleted of these molecules as fast and as efficiently as possible by imaging this ROI with high intensity illumination; (iii) postbleach imaging, i.e. one or several time series under the same conditions as used in the prebleach

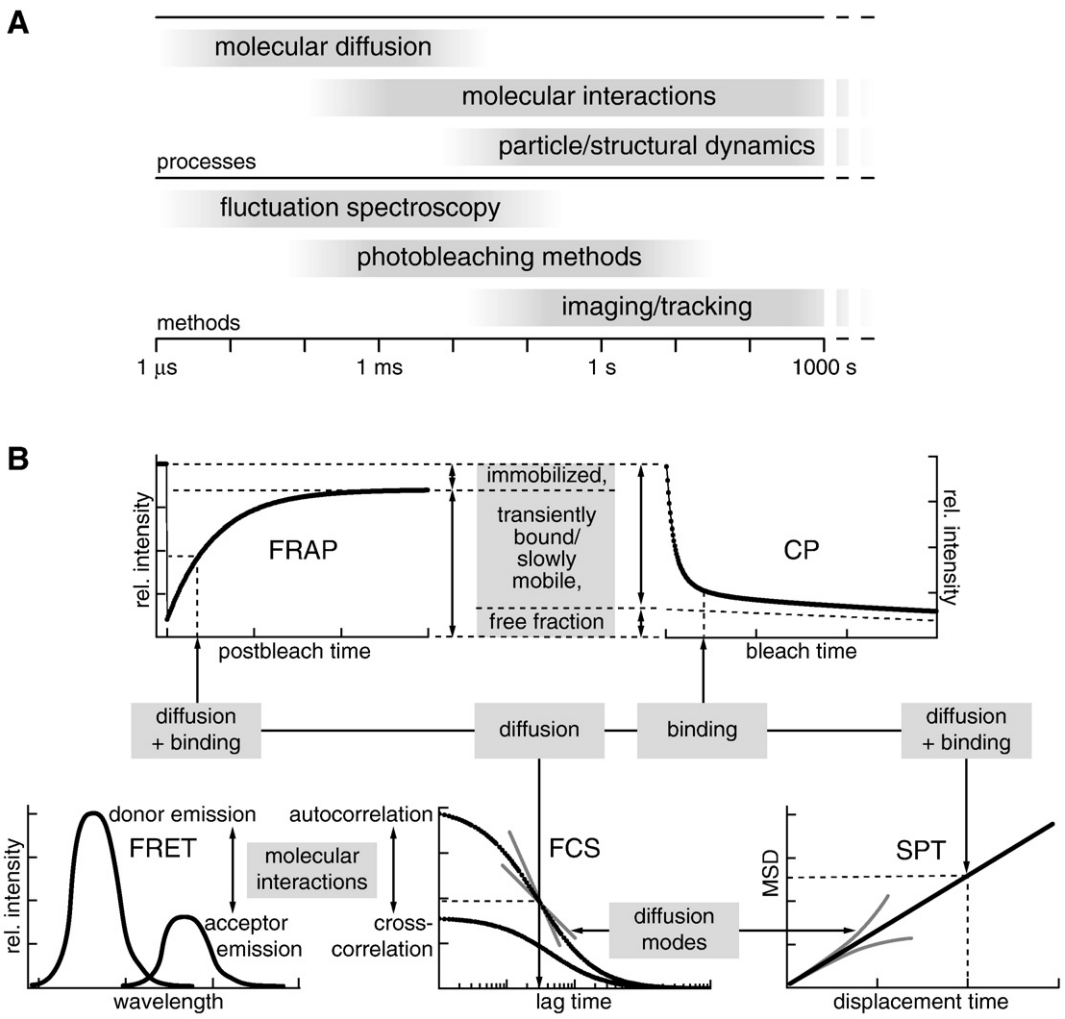

Fig. 6. SPT, FRAP, CP/FLIP, FRET and FCS yield complementary mobility information. (A) The processes that define mobilities (see Fig. 4) take place on different time scales between microseconds and hours. On the other hand, different methods cover different and partly overlapping time regimes. Thus, they provide complementary information and can be combined appropriately. (B) Scheme of SPT, FRAP, CP/FLIP, FRET and FCS to illustrate how the parameters as obtained from the different methods (diffusion coefficient, half-time of recovery, dissociation rate, diffusion correlation time, diffusional mode, degree of association, free, transiently bound/slowly mobile and immobilized fractions) are related.

sequence in order to record the redistribution of labelled molecules back to equilibrium due to transport, diffusion, and more or less transient immobilization.

A widely used quantification method is to average the fluorescence intensity over the ROI, to apply appropriate normalization steps [105] and to plot the intensity as a function of time. The "amount" of bleaching or degree of incomplete bleaching [114], the half-time or time constant of recovery, and the immobile fraction can be determined as empirical parameters (Fig. 6B). They characterize the recovery, independent of the actual processes behind the redistribution of molecules. This is useful when only changes in mobility or binding properties are studied. In order to obtain the actual physical parameters of the processes involved, such as the diffusion coefficient or the dissociation rate, models must be applied that take into consideration Brownian motion, binding and immobilization, cellular topology, and the geometry of the ROI. There are quite a few examples of more or less explicit expressions for the intensity recovering over time [114,131,132]. In the majority of the biological studies, it has been assumed, in order to simplify the analysis, that diffusion could be neglected (e. g. [98,133]). Very often, however, neither diffusion nor binding/immobilization dominate the mobility, and a more detailed spatio-temporal description in combination with numerical modeling of the complete reaction–diffusion scheme is necessary in order to achieve the correct interpretation of the data (see above) [96,97,111,134,135]. Hence, physical parameters like the diffusion coefficient and association and dissociation rates can be extracted from the experimental data. Under certain conditions, it is possible to find an explicit solution [136,137]. In order to restrict the complexity, one can reduce the geometry to two or one effective spatial dimension, assuming that the system has reached equilibrium and considering large structures, that provide binding sites, as immobile [97,111]. This must be controlled and justified in each particular situation. From the full reaction–diffusion model, simplified cases have been derived: the diffusion-dominant, the effective diffusion and the reaction-dominant cases [99].

Imaging-based FRAP is fundamentally limited by the acquisition speed of the microscope used, which provides usually a time resolution well above a millisecond, rendering the identification of real translocation difficult or impossible for diffusion coefficients above 1–10 $\mu m^2\ s^{-1}$. This can be overcome by the alternative or additional use of non-imaging methods such as point FRAP, CP and FCS, especially in the face of subsequent quantitative modeling applied to dissect diffusion and binding processes (see Fig. 6B).

3.4. Continuous fluorescence photobleaching

Continuous fluorescence photobleaching (CP) studies are based on imaging [138], line-scanning [139] or more general geometries. Here,

we will focus on point CP where the focus of a confocal system is fixed at a desired position in a cell and the decrease of fluorescence in the so-defined observation volume is recorded under continuous illumination [140,141]. Gradually, a dynamic equilibrium between association to and dissociation from immobile structures, diffusion/transport, and photobleaching is established. This is represented by a characteristic decay of the fluorescence signal which often shows biphasic behaviour: a fast initial decay mainly from bleaching of an immobilized or slowly mobile/transiently bound fraction and a slow asymptotic decay from bleaching of the whole pool of freely mobile molecules exchanging with the bound fraction. Already qualitatively, one can distinguish the case of fully diffusive from fully immobilised molecules or a mixture (see Fig. 6B) from the curve. A quantitative analysis is feasible since the bleaching and observation volume of a point CP experiment are sufficiently well defined [141]. It yields the different fractions and properties of the binding reaction. Moreover, the focus is small in relation to diffusive translocation so that the conditions for a pseudo-first order approximation of the immobilization reaction (see above) are met in most cases when the bleaching and the dissociation rate are of the same order of magnitude. Especially in combination with FRAP experiments, CP allows to distinguish free, transiently bound, and immobilized fractions without the demand for numerical modeling (Fig. 6B).

3.5. Fluorescence correlation spectroscopy (FCS)

In an FCS experiment, the focus of a confocal laser illumination and fluorescence detection system like that of a confocal microscope defines a small observation volume. It is fixed at a position of interest (Fig. 5), since FCS is not an imaging method. Due to their diffusion fluorescently labelled molecules can enter and leave the focus, resulting in signal fluctuations at the detector. The average lengths and amplitudes of the fluctuations are determined by so-called temporal autocorrelation analysis [105]. Appropriate biophysical models for the sources of fluctuations, see above, allow for example to quantify the concentrations and diffusion coefficients and to distinguish small free proteins from large complexes to which they are bound. Besides diffusion, other sources of fluctuations are photophysical effects such as molecular blinking, interactions with cellular structures, or the movement of these structures themselves. In the simple and frequent case of freely mobile molecules, the major readouts of FCS are the number of molecules and their mean dwell time in the observation volume. Comparing the kinetics of pure diffusion as obtained from FCS to the joint kinetics of diffusion and binding from FRAP data enables to assess the binding contribution without elaborate modeling (Fig. 6B). In a two-color setup (fluorescence cross-correlation spectroscopy, FCCS), potential binding partners are labelled with spectrally different fluorophores [142,143]. When they associate, diffusion generates synchronized fluctuations in different detection channels, which can be quantified by cross-correlation analysis featuring high sensitivity for biomolecular interactions and yielding the fractions of bound and free molecules and other association/dissociation parameters [144,145].

Even reaction–diffusion models containing several exchanging molecular species are analytically applicable to the theoretical framework of FCS, provided that all species are (sufficiently) mobile so that they generate concentration fluctuations and do not show strong photobleaching [116]. The same holds for different diffusion modes, though often difficult to distinguish [121,146,147]: the anomaly parameter α can also be derived from FCS experiments. Finally, as an example for studies on the accessibility of the nuclear interior, FCS can be used to determine the effective size of macromolecules, the hydrodynamic radius *in vitro* (see above and [78]) as well as the intranuclear mobility *in vivo* with very high precision and sensitivity. In a different approach, FCS can be used to calibrate intensity images towards a transformation into real concentration maps of nuclear proteins [77].

3.6. Image correlation spectroscopy

Image correlation spectroscopy (ICS) has been used in various different implementations usually based on a confocal laser scanning microscope: first, spatial rather than temporal fluctuations in the density of molecules, e.g. membrane receptors, were studied using confocal images [148]. As an extension, from a time series of these images, both the spatial and the temporal information can be used for correlation analysis [149]. Recently, the RICS (raster image correlation spectroscopy) technique was introduced which exploits the correlated spatio-temporal information inscribed into confocal images during the scanning process [150]. Conceptually, it provides the same information as conventional FCS, however by abandoning spatial resolution and with some limitation in terms of detecting fast intensity fluctuations.

While any hybrid between FCS and imaging is conceivable, in a somewhat simpler approach ICS can be used as a tool to quantify the average size of randomly organized structures. When conducting an image cross-correlation analysis of two different signals the co- and anti-localization as well as information about the size of structures or objects is obtained, in which differently labeled molecules co-localize or from which they are mutually excluded. In the latter context, ICS was applied to measure the size of subchromosomal high-density areas and their decomposition upon chromatin decondensation [79] and the chromatin accessibility for differently sized macromolecules [78].

3.7. Fluorescence resonance energy transfer

When fluorescence resonance energy transfer occurs, the excitation energy is transferred from an excited donor fluorophore to an acceptor fluorophore by a dipole-dipole interaction within a range of 1–10 nm (Fig. 5) [119,120]. As a “proximity sensor” on length scales of biomolecules, FRET has served widely as tool to study molecular structure, conformational changes and molecular associations both *in vitro* and – more and more in recent years – as contrast-defining signal in cellular imaging [151]. Since it does not involve diffusion processes, it can be used to detect molecular interactions (conceptually complementarily to FCCS) and multimerization processes e.g. due to self-assembly or -organization even of immobile structures.

In addition to the spatial proximity, the emission spectrum of the donor and the absorption spectrum of the acceptor must overlap sufficiently. Different manifestations of FRET in the fluorescence signal of the donor-acceptor system can be used to detect, quantify and image FRET as reviewed previously [152]: (i) with increasing FRET efficiency, the donor emits fewer and the acceptor emits more photons, wich is referred to as sensitized emissions and can be detected with ratiometric dual-channel imaging; (ii) energy transfer provides the donor fluorophore with an additional channel to dissipate excitation energy, so that the occupation of the excited state decays faster and the apparent lifetime of the donor fluorescence decreases; (iii) energy transfer reduces the photobleaching rate of the donor and increases it for the acceptor owing to the corresponding changes in occupation of the respective excited states, or vice versa. Systematic photobleaching of the acceptor reduces the probability for FRET to occur.

4. Dynamics of nuclear components

4.1. Inert molecules and complexes on different scales

From the considerations above, it is apparent that mobility and accessibility of nuclear space are highly dependent on the size of a given particle. As a reference point the 27 kDa green fluorescent protein (GFP) is used. GFP has a barrel-like structure with a diameter of ~3 nm and a height of ~4 nm. It is uniformly distributed

throughout the nucleus in fluorescence microscopy images without any apparent interactions with nuclear structures. The mobility of GFP has been well characterized in a number of studies by means of FCS and FRAP [82,111,121] (Table 1). An averaged diffusion coefficient of 81 $\mu m^2 s^{-1}$ in water at 25 °C with a viscosity of 0.89 mPa s (millipascale second) stands out against a value of $D = 23\ \mu m^2 s^{-1}$ as measured in the cell. The difference can be assigned to an apparent 3.5-fold higher viscosity of the cellular environment. This mobility corresponds to an effective displacement of 12 μm after 1 s, which is similar to the dimensions of the cell nucleus (Table 1). Thus, the time required for an isolated non-interacting protein molecule to "roam" the whole nucleus is in the range of a few seconds, and indeed GFP and Dextrans of similar size have virtually unrestricted access to the whole nucleus. Interestingly, also for larger particles like GFP pentamers with D as small as $8 \pm 1\ \mu m^2 s^{-1}$ no differences in the diffusion coefficients were detected between the cytoplasm and the nucleoplasm [82]. This supports the view that inert particles up to a size of about ~20 nm experience no restriction with respect to their mobility and accessible space in the nucleus during interphase within the diffraction-limited resolution of the fluorescence microscope (Table 1, Fig. 3). In terms of protein mass, these dimensions would correspond to a molecular weight of 2–3 MDa. Accordingly, it is expected that in the absence of interactions with chromatin or other nuclear subcompartments, most nuclear factors are highly mobile. Experimental data that describe their mobility resulting from both diffusion and interactions have been compiled in Table 2. With increasing size, macromolecules and complexes become increasingly excluded from nuclear areas of higher density as could be shown with imaging and ICS [78] while they are still mobile. In contrast, dextrans, nanospheres and inert NB-like complexes larger than 100 nm are trapped locally. However, they show some chromatin-embedded mobility as observed with SPT and FRAP, which is comparable to what was found for chromatin loci themselves as well as for NBs. Data that describe their translocations are given in Table 3.

4.2. Chromatin

4.2.1. Chromosomal proteins and nucleosomes

A number of studies have revealed that structurally relevant proteins such as the core histones [123,153], the centromere proteins CENP-A (a histone variant), CENP-I and CENP-H [154] and cohesins [155] are stably associated with chromatin (Table 2). For the canonical core histones H2A, H2B, H3 and H4 the vast majorities (>90%) have typical residence times of two to more than 8.5 h with a freely mobile fraction of only a few percent. However, a high mobility fraction of H2A·H2B of 3–5% appears to be functionally relevant as its presence can be assigned to transcription [123]. This might be related to a facilitated movement of RNA polymerase through chromatin via the formation of a hexasome particle that has one H2A·H2B dimer missing from the nucleosome [156]. Furthermore, in mouse ES cells an increase of the high mobility fraction of core and linker histones as well as other chromosomal proteins was observed in FRAP measurements [157,158]. This "hyperdynamic" binding of structural chromatin proteins was identified as a functionally important hallmark of pluripotent ES cells. As discussed previously, the relative interaction affinity of chaperones like NAP1 with core and linker histones determines the equilibrium between DNA-bound histones and freely mobile yet chaperone-bound histones (Fig. 1) [29,159,160]. This view is supported by the recent finding that histone chaperones HIRA and NAP1 accumulate in mouse primordial germ cells undergoing reprogramming, which has been related to DNA demethylation via a DNA repair-based mechanism [161]. Furthermore, it has been shown that histone acetylation by the p300 acetyltransferase facilitates the transfer of the H2A·H2B dimer from nucleosomes to NAP1 and is thus expected to render it more mobile [162].

In addition, the activity of ATP-dependent chromatin-remodeling complexes could also affect histone mobility and three aspects need to be considered. (i) The translocation of nucleosomes along the DNA could contribute to an increase of the apparent histone mobility. However, these movements are likely to occur mostly on the length scale defined by the length of the linker DNA and the NRL, i.e. a range of 17 to 67 nm. Under *in vitro* conditions such a movement of an isolated nucleosome along the DNA is completed after 30–60 s [163]. The kinetics of this process in living cells are currently unknown. (ii) As depicted in Fig. 1, chromatin remodeling complexes are essential for establishing a regular spacing of nucleosomes, and therefore are important for nucleosome assembly during replication. The regular spacing is required for folding the chain of nucleosomes into a compact and stable chromatin fiber, which inhibits the chaperone-mediated exchange of core histones [159]. Accordingly, a reduced chromatin remodeling activity at this stage would be also expected to promote turnover between DNA-bound and soluble histones. (iii) Chromatin remodeling activity could directly contribute to the release of core histones from chromatin. This refers to the process of nucleosome eviction [40,41] as well as the activity of chromatin remodeling complexes to exchange canonical and variant core histones [164].

In addition to the above-mentioned stably bound chromosomal proteins (core histones, several centromeric proteins and cohesins) another group of structural chromatin proteins exists that display much higher dynamics. These include the linker histone H1 [124,125], heterochromatin protein 1 (HP1) [165, 166] and high mobility group (HMG) proteins. Their residence times on chromatin are surprisingly short in the order of only a few seconds to minutes. The same appears to be true for chromatin-modifying proteins like the histone methyltransferase Suv39H1 (Table 2).

4.2.2. Genomic loci

The translocation of chromatin loci has been studied by monitoring the mobility of a photobleached spot in dye-labeled chromatin [167] or by tracking fluorescently labeled regions [168,169]. In order to trace individual chromosome loci in living eukaryotic cells, the *lac* operator/LacI-GFP system was introduced by Belmont and co-workers [170], and was widely used to follow translocation and conformational changes of chromatin as reviewed recently [171]. Based mainly on SPT, average apparent diffusion coefficients of $1–2 \cdot 10^{-4}\ \mu m^2 s^{-1}$ have been reported for chromatin loci and for large nuclear particle movements within a corral of 200–300 nm radius that can translocate in the nucleus as part of larger chromatin domains [172] (Table 3). These relatively slow and confined movements are in agreement with a territorial organization of chromosomes and consistent with the slow mobility of chromatin ends formed after introducing a DNA cut [173]. However, although the mobility of most chromatin loci appears to be quite restricted, long-range movements have been reported under certain conditions [174], and are important in the context of transcription-related chromatin reorganization [6–8].

4.3. Transcription, replication and DNA repair complexes

Transcription, replication and DNA repair share a number of features in terms of their dynamics and assembly properties [6]. Many subunits involved in these processes bind with a high turnover rate from a freely mobile fraction with average chromatin residence times of only a few seconds (Table 2). In the context of transcription, this highly dynamic binding has been demonstrated for the binding of gene-specific transcription factors [175] as well as for initiation of the RNA polymerase I and II transcription machineries themself [133,176,177]. However, a rapid binding and dissociation equilibrium is not shared for all steps and factors involved in transcription. For example the binding of the heat shock protein (HSP) transcription factor in *Drosophila* shows a fast mobility at chromosomal loci under

Table 2
Mobility and interaction parameters of nuclear proteins and RNAs

Molecule	$t_{1/2}$ (s)	D_{app} (μm^2 s^{-1})	t_{res}	References
Core histones H2A, H2B, H3, H4[a]				
Highly mobile		10–20		[77,123,153]
Slowly mobile H2A·H2B fraction	360			
Immobile[b]			2 h, >8.5 h	
Linker histone H1[a]				
Mobile		0.01	~1 s	[96,111,124,125,238]
Slowly mobile			120–220 s	
Heterochromatin protein HP1[a]				
Highly mobile	0.6–1			[165,166,239–241]
Slowly mobile	4–15	0.6–0.7		
Immobile	>60			
Histone methyltransferase Suv39H1				
Mobile[c]	11–19		~1 s	[111,240]
Slowly mobile	>420			
Polycomb complex				
Mobile (CBX, average)	10–40			[228,229]
Mobile (pcg complex)		0.2–0.7		
Slowly mobile (Ph, Pc in pcg)			2–6 min	
Centromeric proteins				
Mobile (nucleoplasmatic)		0.08–3		[154]
Slowly mobile (CENP-H)			75 min	
Immobile (CENP-A, -I, -) [b]			>4 h	
HMG proteins				
Highly mobile			4–5 s	[98,195]
Mobile		0.45	25 s	
DNA replication proteins				
Highly mobile (PCNA)		11–15		[180–182]
Mobile (ligase, Fen1)	5			
Slowly mobile (PCNA)	90			
DNA repair proteins XP-A,-B,-C,-G, DDB2,ERCC1,bparg103				
Highly mobile (undamaged cells)	1–10	2–28		[183–186]
Slowly mobile (DNA damage)			>4 min	
Cohesin				
Slowly mobile			25 min	[155]
Immobile [b]			>6 h	
RNA polymerase I factors				
Mobile			0.2–1.4 s	[133]
Slowly mobile			120–181 s	
RNA polymerase II factors				
Mobile (promoter bound)	15		6 s	[176,177]
Mobile (initiation)			54 s	
Slowly mobile (elongating)	1200		9 min	
TFIIH				
Mobile (RNA pol I)			25 s	[188]
Mobile (RNA pol II)			6 s	
Slowly mobile (DNA repair)			4 min	
Splicing factors U2AF65, SC35, SF1, Y14, SF2/ASF				
Highly mobile[c]	0.2–0.4	0.5–1.4		[194–196,198]
Mobile (SF2/ASF)	10–25	0.2		
Slowly mobile	>60			
Polyadenylated mRNA				
Mobile[c]		0.3–0.7		[122,199]
Slowly mobile		0.03–0.04		
Cajal body protein coilin				
Mobile		0.3–0.4		[201]
Slowly mobile			15 s-35 min	

Table 2 *(continued)*

Molecule	$t_{1/2}$ (s)	D_{app} (μm^2 s^{-1})	t_{res}	References
PML body protein PML				
Mobile		1–3		[202]
Slowly mobile (PML I-IV, VI)			4–9 min	
Immobile (PML V)			48 min	

The parameter $t_{1/2}$ is the half-time of recovery from FRAP experiments, D_{app} stands for the apparent diffusion coefficient and t_{res} is the average residence time at binding sites.
[a] Variants/isoforms are not considered separately.
[b] This fraction is essentially immobile and does not exchange on the hour time scale. The increase of fluorescence recovery is due to loading of the protein to newly created binding sites during DNA replication.
[c] Differences are dependent on nuclear localization.

non-heat shock conditions ($t_{1/2}$=15 s) but a much slower exchange after heat shock with $t_{1/2}$>5 min [178]. In addition, once the RNA polymerase I or II complex has completed the initiation phase, the polymerase complex remains stably associated during transcript elongation for average times of 2–3 min (RNA polymerase I [133]) or 9–20 min (RNA polymerase II [176,177]).

The prevalence of stochastic (dis)assembly events observed in transcription appears to be also characteristic for replication and DNA repair as discussed previously [179]. Replication complexes exist for several minutes, resolve and reassemble from freely mobile factors [180–182]. Similarly, DNA repair loci form in a very dynamic manner from nucleoplasmic components as studied for DNA double strand breaks and nucleotide excision repair pathways [183–187]. After the induction of a DNA damage site, some subunits display a sequential binding with very different kinetic rates while others appear to bind independently with indistinguishable kinetics [183,185–187] (Table 2). Furthermore, some proteins like transcription factor II H (TFIIH) are also involved in multiple cellular processes [188]. This points to a complex protein-DNA and protein-protein interaction network that integrates stochastic binding of multiple subunits into the assembly of a defined supramolecular complex.

4.4. mRNA and mRNA-processing complexes

The export of messenger RNA (mRNA) from the nucleus into the cytoplasm is preceded by mRNA splicing in distinct multi-subunit mRNA-protein complexes (mRNPs). Splicing involves uridine-rich small nuclear ribonucleo-protein particles (snRNPs) as well as a large number of proteins, which associate to the so-called spliceosome [189]. The spliceosome undergoes several rearrangements in the course of splicing by forming intermediate complexes, which carry out the major catalytic steps, i.e. excision of introns and ligation of exons. At the same time, factors required for translation, quality control and export are recruited to the mRNA. These proteins associate with the mRNA forming the so-called exon–exon junction complex (EJC) [190]. The composition of the spliceosome/RNA and EJC/RNA complexes has been well characterized on the biochemical level [191–193]. Various splicing-related factors bind already co-translationally and almost all of them including the mRNA accumulate in discrete nuclear clusters termed speckles or SC35 domains [15]. Spliceosome and EJC components (tagged with fluorescent proteins) as well as mRNA (labeled via hybridization of tagged oligo(dT) to the poly (A) tail) show a surprisingly high mobility throughout the whole nucleus [122,194–196] with apparent diffusion coefficients between 0.24 and 1.4 μm^2 s^{-1} as obtained with FRAP and FCS (Table 2). This is one to two orders of magnitude slower than free GFP and in the expected range for large diffusive mRNPs within chromatin. More detailed studies using FCS, FRAP and CP suggest that EJC proteins are present in free fractions as well as integrated into mobile yet mRNA-associated complexes. Mainly in nuclear speckles, additional short- and long-term immobilization occurs in a protein-specific and RNA-dependent way [197,198]. The mRNA is found in a slowly mobile state with a diffusion coefficient of 0.03–0.04 μm^2 s^{-1} [199]. Thus, the assembly of mRNA-processing complexes seems to be highly dynamic and randomly organized, with their constituents being in a continuous exchange with a nucleoplasmic pool, which is not only present in nuclear speckles. However, the catalytic steps of splicing and the actual nuclear export require the complete and at least transiently stable assembly of highly specific complexes of splicing, EJC, and export factors on the mRNA.

Table 3
Mobility of chromatin loci and nuclear bodies in the nucleus

Particle	D [μm^2 s^{-1}]	r_c [nm]	References
Cajal bodies[a]	$1.1{\cdot}10^{-4}$	280	[85]
PML bodies[a]	$1.2{\cdot}10^{-4}$	310	[85]
Euchromatin[b]	$1.3{\cdot}10^{-4}$	150	[203]
Chromatin[c]	$2.4{\cdot}10^{-4}$	150	[207]
Telomeres[d]	$1.8{\cdot}10^{-4}$	240	[204]
Heterochromatin	$4.8{\cdot}10^{-5}$	230	[85]
1 Mb chromatin domain	$0.5–1.5{\cdot}10^{-5}$	180	[242]

D is the diffusion coefficient and r_c is the radius of confinement, i.e. the effective radius of the region, within which a given particle or chromatin locus can translocate its center of mass during an observation time of up to a few minutes.
[a] The given diffusion coefficient refers to the value D_c according to Eq. (4), which is believed to reflect the mobility of the chromatin environment.
[b] A *lac*O array with integration site 5p14 was studied, which corresponds to a G band with a preferred localization in the interior of the nucleoplasm.
[c] The locus displacement occurred in 150 nm jumps that lasted 0.3–2 s. The given D value refers to the slower free diffusive contribution detected on the seconds time scale.
[d] This is the value observed for the majority of telomeres. A ~10% fraction of telomeres showed a higher mobility with a diffusion coefficient of D=$5.8{\cdot}10^{-4}$ μm2 s^{-1}.

4.5. Nuclear bodies

Nuclear bodies or subcompartments are dynamic with respect to the exchange of their constituting components as well as in their translocations within the nucleus. In general, the constituting protein components are in a fast exchange with the nucleoplasm on the scale of seconds to minutes as shown for the nucleolus [13,200], CBs [201], PML-NBs [202] and speckles [13,15] (Table 2). An exception is the high residence time of 48 min reported for the exchange of the PML V splicing variant between the freely mobile state in the nucleoplasm and the PML-NB complex, suggesting that it provides a more stable structural scaffold for the other mobile components [202].

For CBs and PML-NBs, their translocation within the nucleus reflects features of the chromatin environment (Table 3). On the time scale of a few minutes or less, their movements can be described by a diffusion-like motion of the particles' center of mass in a corral with a radius of 200 to 300 nm. This value is strikingly similar to the region in which chromatin loci themselves display a random movement. Furthermore, the chromatin locus mobility over larger distances occurs with an apparent diffusion coefficient of up to ~10^{-4} μm^2 s^{-1} [85,203,204]. Accordingly, it was proposed that the dynamic chromatin organization of the interphase nucleus determines the confined translocation of mobile nuclear subcompartments like PML and Cajal bodies, and their targeting to certain regions of the nucleus [85,172]. It is noted that the apparent mobility of nuclear bodies as described by their diffusion coefficient and accessible space is highly dependent on the observation period, as both parameters are affected by the different levels of chromatin organization. Consistent with this view, the mobility of chromatin loci itself shows various scales of

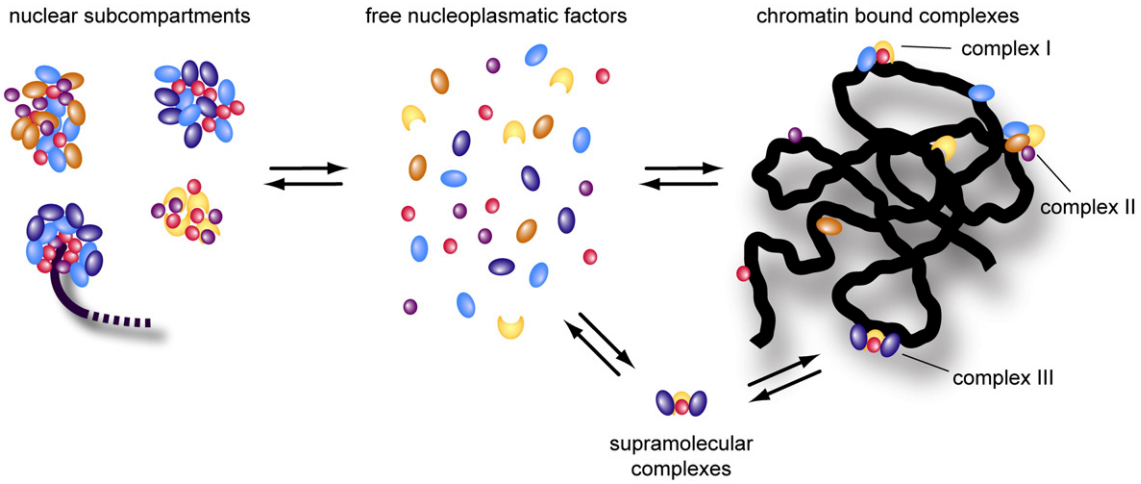

Fig. 7. Highly dynamic macromolecular interactions in the nucleus. The available data on the dynamics of genome organization point to its dynamic compositions and a continuous and reversible turnover of macromolecules in the nucleus between different states. These include the association into various nuclear subcompartments, a free, highly mobile state in the nucleoplasm, the presence of preassembled supramolecular complexes as well as various chromatin-bound states.

movements as inferred from the analysis of different time regimes [171,205–207]. While the above description of the mobility of PML-NBs and CBs as a function of the accessibility and dynamics of its chromatin environment (similar to that of an inert particle of similar size) gives a very good agreement with experimental data, it is clearly questionable for situations in which these subcompartments are in a chromatin-bound state. In particular, it has been shown that Cajal bodies are associated to several different snRNA and snoRNA (small nuclear/nucleolar RNA) gene loci as well as histone gene loci [208–212]. For PML-NBs an occasional association to certain gene regions [213,214] as well as the formation of specific complexes with telomeres [215] has been reported. It is noted that an alternative mechanism for the translocation of nuclear bodies would be a highly dynamic fluid-like conformation that allows a transient disruption of its structure during passage through chromatin as it appears to be the case for nuclear speckles/SC35 domains [216].

5. Dynamic genome organization versus specific nuclear activities

5.1. Mobility differences of nuclear factors

The data reviewed here demonstrate that many nuclear proteins are present as a highly dynamic fraction. They diffuse rapidly throughout the nucleoplasm with FRAP recovery half-times in the order of a few seconds and diffusion coefficients around 10 $\mu m^2\ s^{-1}$ (Table 2, [96,98,141,217–219]). Furthermore, a number of apparently static supramolecular structures experience a continuous and reversible turnover of their components. This refers to the transient binding of a fraction of chromosomal proteins like HP1 and linker histones or several RNA polymerase I and II transcription factors. These transient interactions are characterized by apparent diffusion coefficients around 1 $\mu m^2\ s^{-1}$ and average residence times of 1–30 s. This view is depicted schematically in Fig. 7. Upon inspection of the data

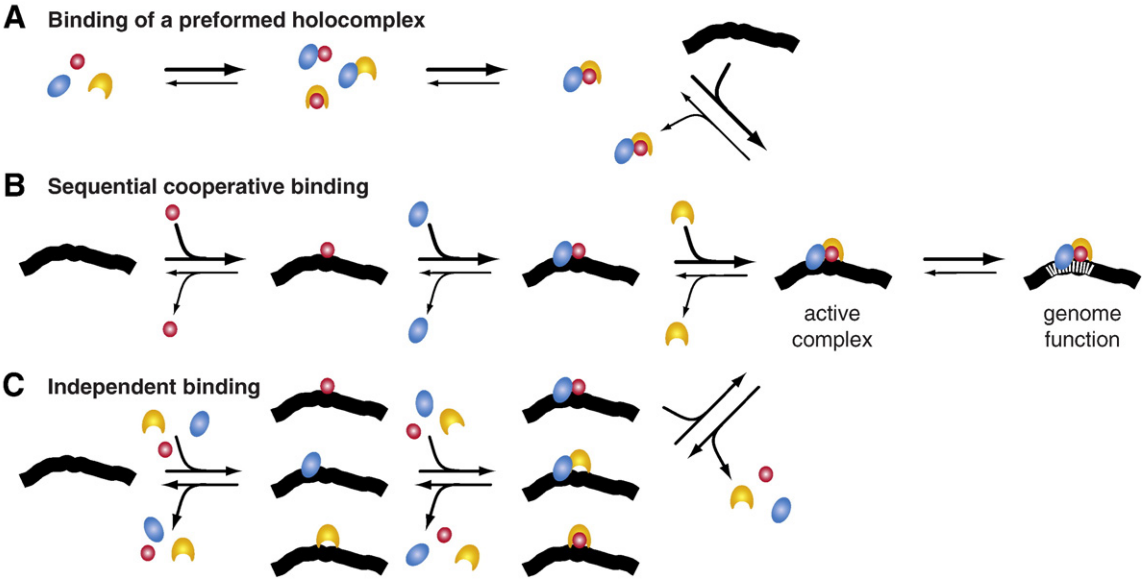

Fig. 8. Reaction pathways for assembly and binding of genome-modifying complexes. Three mechanistically different pathways for the formation of a multi-subunit genome-modifying complex can be distinguished. Once the complete active complex is assembled, the (transient) genome function reaction (post-translational histone or DNA modification, transcription, replication etc.) proceeds to a new state in an essentially irreversible reaction. In general, this state can be reversed via the activity of another complex. (A) The subunits assemble already into a complete complex in the nucleoplasm, which then binds to chromatin. (B) The complex is assembled on its chromatin target via cooperative binding of factors, so that chromatin binding occurs in a predetermined sequential order. (C) Chromatin binding of subunits can occur independent of each other to give rise to a high number of incomplete intermediate states, all of which can be further augmented to the complete active complex.

compiled in Table 2, it is also apparent that a number of species exists, of which a relatively immobile bound protein fraction displays average residence times of minutes, while a fourth group is essentially immobile on the hour time scale. The latter class is represented by core histones, several centromeric proteins and cohesins that provide the structural framework for a stable genome structure.

As pointed out previously, many aspects of the dynamic structure of the genome and its interacting nuclear subcompartments have features of self-organizing entities. Owing to the intrinsic properties of their components, they assemble into distinct structures [6,12,68,220–223]. These maintain their ability to rearrange into different functional states as evident from the fast exchange of protein components with the nucleoplasm. The macroscopic properties are determined by the interactions and properties of the components that can be tuned for example by post-translational modifications like phosphorylation, acetylation, methylation and sumoylation. The assembly exploits stochastic fluctuations of its components and does not require any template or framework. This results in a broad spectrum of molecular mobilities that requires a complementary set of fluorescence fluctuation microscopy methods to be captured experimentally (Fig. 6). In the context of the formation of nuclear subcompartments, self-organization has been suggested to drive the assembly of the nucleolus [13,200], of nuclear speckles/SC35 domains [13,15], of CBs [201] and PML-NBs [224,225], and of transcription and replication factories [6,12]. It can be facilitated substantially by molecular crowding where the thermodynamically unfavorable gain of order for the emerging complexes is overcompensated by the entropy gain of all soluble molecules [28]. The concept of self-organization clearly serves to rationalize the plasticity of genome organization as well as many macromolecular interactions in the nucleus. However, one might ask to which extent it is also suited to fulfill the requirements of stability and specificity of the genome-related activities.

5.2. Mechanisms of complex assembly in the nucleus

To address the questions raised above it is instructive to consider mechanistic differences with respect to the interactions of nuclear factors. Genome functions as for example the synthesis of an mRNA transcript or its export out of the nucleus are essentially irreversible reactions towards a new cellular state, and as such ensure specificity. Thus, for a multi-subunit complex that exerts a specific genome-related function, the relevant mechanistic differences occur during the steps that lead to the assembly of the active complex. For the formation of such a complex, (at least) three principal mechanisms can be distinguished that are depicted in Fig. 8.

5.2.1. Binding of a preformed holocomplex (Fig. 8A)

The subunits are present as an already assembled complete complex in the nucleoplasm. In the presence of a competent chromatin state, the holocomplex can bind and then conduct a genome-modifying reaction. Complexes of this type can reach a size of 2–3 MDa as for example the human RNA polymerase II holoenzyme [226] or the SWI/SNF [227] and Polycomb chromatin remodeling/modifying complexes [228,229]. It is noted that these complexes can display various degrees of subunit exchange between the holocomplex and free subunits in the nucleoplasm.

Table 4
Comparison of pathways for formation of an active complex at chromatin

	Binding of a holocomplex (Fig. 8A)	Sequential cooperative binding (Fig. 8B)	Independent binding (Fig. 8C)
Stability	High	High	Low
Plasticity	Low	Low	High

5.2.2. Sequential cooperative binding (Fig. 8B)

In this scheme, the complex is assembled in a defined sequence on its chromatin target via cooperative binding of factors. The cooperative binding of subunits ensures that incomplete intermediates are depleted, i. e. the dissociation rate from each state is low. This drives the reaction in the direction of the complete complex. An example for this type of pathway would be the histone chaperone-mediated assembly of a nucleosome, which proceeds via the sequential formation of a tetrasome (histone H3·H4 tetramer bound to the DNA) and a hexasome (complex of DNA, H3·H4 tetramer and one H2A·H2B dimer) particle. The sequential order of this process can be described quantitatively *in vitro* on the basis of differences in the reaction equilibria of the intermediates [29,160].

5.2.3. Independent binding (Fig. 8C)

Chromatin binding of subunits can occur independently from each other to give rise to a high number of incomplete intermediate states, all of which can be further augmented to the complete active complex. Once the complete active complex is assembled, it is stabilized in an “engagement”-like manner to conduct a genome-associated function. An example for a pathway that is dominated by this type of assembly is the mammalian polymerase I transcription initiation complex, which displays a highly dynamic independent stochastic binding of subunits [133]. Similarly, for RNA polymerase II initiation it was concluded that transcription initiation proceeds via a diffusion-driven fast binding and dissociation equilibrium of the polymerase and other factors at the promoter that only occasionally reaches a complete transcriptionally competent complex state [176,177]. A stochastic (dis)assembly process is not unique for transcription initiation but was also observed for two different DNA repair pathways as discussed previously [179]. In addition, a recent comprehensive study in living cells on the kinetics of protein complex assembly in nucleotide excision repair demonstrates that several subunits are binding independently to the repair sites (M. Luijsterburg, G. von Bornstaedt, T. Höfer and R. van Driel, personal communication).

5.3. Conclusions

Evaluating the above-mentioned reaction pathways in terms of their compatibility with stability and plasticity, a simplified classification as presented in Table 4 can be proposed. It is apparent that the formation of a stable complex of defined composition and specific function contradicts plasticity and the multifunctional use of subunits. The latter appears to be an advantage of the independent binding mechanism, in which the same subunits can be exchanged between different functional states. One example is the TFIIH helicase, which is engaged in RNA polymerase I and II transcription as well as in DNA repair [188]. On the other hand, the assembly of a multi-subunit state by a series of reversible independent binding events will lead to the coexistence of multiple incomplete intermediates that are likely to display various residual activities (Fig. 8C). This state and its potentially harmful side-reactions are avoided for a pre-existing stable complex (Fig. 8A), for which specificity depends on the preferential recognition of its target site over other genomic loci. Furthermore, the simultaneous existence of a number of intermediate states could make the formation of the complete and fully functional complex a very slow process. Any differences in the rate of functional complex assembly via sequential cooperative binding as compared to an independent binding mechanism will depend on a number of parameters like the degree of reversibility of the single binding steps, the number of subunits involved as well as their concentration. Thus, specific cases need to be considered in quantitative models if one attempts to draw conclusions on the kinetic effects of these mechanistic differences.

In the cell any combination of the three scenarios shown in Fig. 8 can be implemented. This is illustrated for the case of transcription

initiation of yeast RNA polymerase II, a well studied complex multi-step reaction. The complete initiation complex that assembles at the promoter contains ~60 protein subunits and has a molecular weight of ~3 MDa [230,231]. It consists essentially of three components, the 12 subunit RNA polymerase II, 26 general transcription factors and a "mediator" complex comprising 21 subunits. RNA polymerase II is a 515 kDa complex that is present as 10-subunit stable catalytic holoenzyme core and the dissociatable Rpb4/7 heterodimer. At the promoter, the polymerase serves as the platform for binding of general transcription factors (TFIIB, -D, -E, -F, -H and -A) and the mediator complex. This assembly proceeds via a mixture of sequential cooperative and independent binding steps until the state is reached from which transcription can start [231–233]. Similarly, a combination of binding of preformed complexes in conjunction with stochastic as well as cooperative assembly of the active complex can be identified in chromatin organization, transcription, RNA processing, DNA replication and repair as discussed above. Such a combination of different assembly mechanisms could serve to tune the system between flexible and multifunctional use of its components on the one hand and fast and specific transitions to new functional cell states on the other hand.

Acknowledgements

This work was supported by DFG grant Ri 828/5-3 to KR and a grant of the Christiane Nüsslein-Volhard Foundation to MCH. We are grateful to Harald Herrmann-Lerdon and Peter Hemmerich for comments.

References

[1] S. Yamanaka, Pluripotency and nuclear reprogramming, Philosophical transactions of the Royal Society of London 363 (2008) 2079–2087.
[2] S.D. Taverna, H. Li, A.J. Ruthenburg, C.D. Allis, D.J. Patel, How chromatin-binding modules interpret histone modifications: lessons from professional pocket pickers, Nat. Struct. Mol. Biol. 14 (2007) 1025–1040.
[3] T. Kouzarides, Chromatin modifications and their function, Cell 128 (2007) 693–705.
[4] P. Jones, S. Baylin, The epigenomics of cancer, Cell 128 (2007) 683–692.
[5] P.P. Amaral, M.E. Dinger, T.R. Mercer, J.S. Mattick, The eukaryotic genome as an RNA machine, Science 319 (2008) 1787–1789.
[6] T. Misteli, Beyond the sequence: cellular organization of genome function, Cell 128 (2007) 787–800.
[7] C. Lanctôt, T. Cheutin, M. Cremer, G. Cavalli, T. Cremer, Dynamic genome architecture in the nuclear space: regulation of gene expression in three dimensions, Nat. Rev. Genet. 8 (2007) 104–115.
[8] P. Fraser, W. Bickmore, Nuclear organization of the genome and the potential for gene regulation, Nature 447 (2007) 413–417.
[9] T. Sexton, H. Schober, P. Fraser, S.M. Gasser, Gene regulation through nuclear organization, Nat. Struct. Mol. Biol. 14 (2007) 1049–1055.
[10] E.C. Schirmer, R. Foisner, Proteins that associate with lamins: many faces, many functions, Exp. Cell Res. 313 (2007) 2167–2179.
[11] A. Akhtar, S.M. Gasser, The nuclear envelope and transcriptional control, Nat. Rev. Genet. (2007) 1471-0056.
[12] P. Cook, The organization of replication and transcription, Science 284 (1999) 1790–1795.
[13] K. Handwerger, J. Gall, Subnuclear organelles: new insights into form and function, Trends Cell Biol. 16 (2006) 19–26.
[14] R. Bernardi, P.P. Pandolfi, Structure, dynamics and functions of promyelocytic leukaemia nuclear bodies, Nat. Rev. Mol. Cell. Biol. 8 (2007) 1006–1016.
[15] A.I. Lamond, D.L. Spector, Nuclear speckles: a model for nuclear organelles, Nat. Rev. Mol. Cell. Biol. 4 (2003) 605–612.
[16] K.E. van Holde, Chromatin, Springer, Heidelberg, 1989.
[17] J.C. Hansen, Conformational dynamics of the chromatin fiber in solution: determinants, mechanisms, and functions, Annu. Rev. Biophys. Biomol. Struct. 31 (2002) 361–392.
[18] C.L. Woodcock, Chromatin architecture, Curr. Opin. Struct. Biol. 16 (2006) 213–220.
[19] P.J. Robinson, D. Rhodes, Structure of the '30nm' chromatin fibre: a key role for the linker histone, Curr. Opin. Struct. Biol. (2006).
[20] S.E. Gerchman, V. Ramakrishnan, Chromatin higher-order structure studied by neutron scattering and scanning transmission electron microscopy, Proc. Natl. Acad. Sci. U.S.A. 84 (1987) 7802–7806.
[21] R. Ghirlando, G. Felsenfeld, Hydrodynamic studies on defined heterochromatin fragments support a 30-nm fiber having six nucleosomes per turn, J. Mol. Biol. 376 (2008) 1417–1425.
[22] G. Dellaire, R.W. Ching, H. Dehghani, Y. Ren, D.P. Bazett-Jones, The number of PML nuclear bodies increases in early S phase by a fission mechanism, J. Cell Sci. 119 (2006) 1026–1033.
[23] A. Pombo, Advances in imaging the interphase nucleus using thin cryosections, Histochem. Cell Biol. 128 (2007) 97–104.
[24] A. Rego, P.B. Sinclair, W. Tao, I. Kireev, A.S. Belmont, The facultative heterochromatin of the inactive X chromosome has a distinctive condensed ultrastructure, J. Cell Sci. 121 (2008) 1119–1127.
[25] K. Handwerger, J. Cordero, J. Gall, Cajal bodies, nucleoli, and speckles in the Xenopus oocyte nucleus have a low-density, sponge-like structure, Mol. Biol. Cell 16 (2005) 202–211.
[26] B. Morelle, J.M. Salmon, J. Vigo, P. Viallet, Measurement of intracellular magnesium concentration in 3T3 fibroblasts with the fluorescent indicator Mag-indo-1, Anal. Biochem. 218 (1994) 170–176.
[27] B.J. Zeskind, C.D. Jordan, W. Timp, L. Trapani, G. Waller, V. Horodincu, D.J. Ehrlich, P. Matsudaira, Nucleic acid and protein mass mapping by live-cell deep-ultraviolet microscopy, Nat. Methods 4 (2007) 567–569.
[28] M. Richter, M. Nessling, P. Lichter, Macromolecular crowding and its potential impact on nuclear function, Biochim. Biophys. Acta 1783 (2008) 2099–2106.
[29] K. Rippe, J. Mazurkiewicz, N. Kepper, Interactions of histones with DNA: nucleosome assembly, stability and dynamics, in: R.S. Dias, B. Lindman (Eds.), DNA interactions with polymers and surfactants, Wiley, London, 2008, pp. 135–172.
[30] J.J. Wyrick, F.C. Holstege, E.G. Jennings, H.C. Causton, D. Shore, M. Grunstein, E.S. Lander, R.A. Young, Chromosomal landscape of nucleosome-dependent gene expression and silencing in yeast, Nature 402 (1999) 418–421.
[31] P.B. Becker, W. Horz, ATP-dependent nucleosome remodeling, Annu. Rev. Biochem. 71 (2002) 247–273.
[32] D.E. Schones, K. Cui, S. Cuddapah, T.Y. Roh, A. Barski, Z. Wang, G. Wei, K. Zhao, Dynamic regulation of nucleosome positioning in the human genome, Cell 132 (2008) 887–898.
[33] S. Henikoff, Nucleosome destabilization in the epigenetic regulation of gene expression, Nat. Rev. Genet. 9 (2008) 15–26.
[34] A. Thastrom, P.T. Lowary, H.R. Widlund, H. Cao, M. Kubista, J. Widom, Sequence motifs and free energies of selected natural and non-natural nucleosome positioning DNA sequences, J. Mol. Biol. 288 (1999) 213–229.
[35] E. Segal, Y. Fondufe-Mittendorf, L. Chen, A. Thastrom, Y. Field, I.K. Moore, J.P. Wang, J. Widom, A genomic code for nucleosome positioning, Nature 442 (2006) 772–778.
[36] I.P. Ioshikhes, I. Albert, S.J. Zanton, B.F. Pugh, Nucleosome positions predicted through comparative genomics, Nat. Genet. 38 (2006) 1210–1215.
[37] H.E. Peckham, R.E. Thurman, Y. Fu, J.A. Stamatoyannopoulos, W.S. Noble, K. Struhl, Z. Weng, Nucleosome positioning signals in genomic DNA, Genome Res. 17 (2007) 1170–1177.
[38] J.L. Gutierrez, M. Chandy, M.J. Carrozza, J.L. Workman, Activation domains drive nucleosome eviction by SWI/SNF, EMBO J. 26 (2007) 730–740.
[39] I. Whitehouse, T. Tsukiyama, Antagonistic forces that position nucleosomes in vivo, Nat. Struct. Mol. Biol. 13 (2006) 633–640.
[40] J.L. Workman, Nucleosome displacement in transcription, Genes Dev. 20 (2006) 2009–2017.
[41] B.R. Cairns, Chromatin remodeling: insights and intrigue from single-molecule studies, Nat. Struct. Mol. Biol. 14 (2007) 989–996.
[42] K. Rippe, A. Schrader, P. Riede, R. Strohner, E. Lehmann, G. Langst, DNA sequence- and conformation-directed positioning of nucleosomes by chromatin-remodeling complexes, Proc. Natl. Acad. Sci. U.S.A. 104 (2007) 15635–15640.
[43] K. Luger, Dynamic nucleosomes, Chromosome Res. 14 (2006) 5–16.
[44] T. Schalch, S. Duda, D.F. Sargent, T.J. Richmond, X-ray structure of a tetranucleosome and its implications for the chromatin fibre, Nature 436 (2005) 138–141.
[45] P.J. Robinson, L. Fairall, V.A. Huynh, D. Rhodes, EM measurements define the dimensions of the "30-nm" chromatin fiber: evidence for a compact, interdigitated structure, Proc. Natl. Acad. Sci. U.S.A. 103 (2006) 6506–6511.
[46] J.R. Daban, A. Bermudez, Interdigitated solenoid model for compact chromatin fibers, Biochemistry 37 (1998) 4299–4304.
[47] J. Bednar, R.A. Horowitz, S.A. Grigoryev, L.M. Carruthers, J.C. Hansen, A.J. Koster, C. L. Woodcock, Nucleosomes, linker DNA, and linker histone form a unique structural motif that directs the higher-order folding and compaction of chromatin, Proc. Natl. Acad. Sci. U.S.A. 95 (1998) 14173–14178.
[48] A. Hamiche, P. Schultz, V. Ramakrishnan, P. Oudet, A. Prunell, Linker histone-dependent DNA structure in linear mononucleosomes, J. Mol. Biol. 257 (1996) 30–42.
[49] N. Kepper, D. Foethke, R. Stehr, G. Wedemann, K. Rippe, Nucleosome geometry and internucleosomal interactions control the chromatin fiber conformation, Biophys. J. 94 (2008) (advance online publication, 22 January 2008).
[50] R. Stehr, N. Kepper, K. Rippe, G. Wedeman, The effect of the nucleosome interaction potential on the folding of the chromatin fiber, Biophys. J. (2008) (advance online publication, 25 July 2008).
[51] M.G. Poirier, M. Bussiek, J. Langowski, J. Widom, Spontaneous access to DNA target sites in folded chromatin fibers, J. Mol. Biol. (2008).
[52] T. Cremer, M. Cremer, S. Dietzel, S. Muller, I. Solovei, S. Fakan, Chromosome territories — a functional nuclear landscape, Curr. Opin. Cell Biol. 18 (2006) 307–316.
[53] W.G. Müller, D. Rieder, G. Kreth, C. Cremer, Z. Trajanoski, J.G. McNally, Generic features of tertiary chromatin structure as detected in natural chromosomes, Mol. Cell. Biol. 24 (2004) 9359–9370.
[54] B.A. Hamkalo, J.B. Rattner, Folding up genes and chromosomes, Q. Rev. Biol. 55 (1980) 409–417.
[55] K.J. Pienta, D.S. Coffey, A structural analysis of the role of the nuclear matrix and DNA loops in the organization of the nucleus and chromosome, J. Cell Sci. (Suppl. 1) (1984) 123–135.
[56] C. Münkel, R. Eils, S. Dietzel, D. Zink, C. Mehring, G. Wedemann, T. Cremer, J. Langowski, Compartmentalization of interphase chromosomes observed in simulation and experiment, J. Mol. Biol. 285 (1999) 1053–1065.

[57] A.L. Paul, R.J. Ferl, Higher-order chromatin structure: looping long molecules, Plant Mol. Biol. 41 (1999) 713–720.
[58] R.K. Sachs, G. van den Engh, B. Trask, H. Yokota, J.E. Hearst, A random-walk/giant-loop model for interphase chromosomes, Proc. Natl. Acad. Sci. U.S.A. 92 (1995) 2710–2714.
[59] J. Sedat, L. Manuelidis, A direct approach to the structure of eukaryotic chromosomes, Cold Spring Harb Symp. Quant. Biol. 42 Pt 1 (1978) 331–350.
[60] A.S. Belmont, K. Bruce, Visualization of G1 chromosomes: a folded, twisted, supercoiled chromonema model of interphase chromatid structure, J. Cell Biol. 127 (1994) 287–302.
[61] T. Tumbar, G. Sudlow, A.S. Belmont, Large-scale chromatin unfolding and remodeling induced by VP16 acidic activation domain, J. Cell Biol. 145 (1999) 1341–1354.
[62] P. Lichter, T. Cremer, J. Borden, L. Manuelidis, D.C. Ward, Delineation of individual human chromosomes in metaphase and interphase cells by in situ suppression hybridization using recombinant DNA libraries, Hum. Genet. 80 (1988) 224–234.
[63] D. Pinkel, J. Landegent, C. Collins, J. Fuscoe, R. Segraves, J. Lucas, J. Gray, Fluorescence in situ hybridization with human chromosome-specific libraries: detection of trisomy 21 and translocations of chromosome 4, Proc. Natl. Acad. Sci. U.S.A. 85 (1988) 9138–9142.
[64] T. Cremer, A. Kurz, R. Zirbel, S. Dietzel, B. Rinke, E. Schrock, M.R. Speicher, U. Mathieu, A. Jauch, P. Emmerich, H. Scherthan, T. Ried, C. Cremer, P. Lichter, Role of chromosome territories in the functional compartmentalization of the cell nucleus, Cold Spring Harb Symp. Quant. Biol. 58 (1993) 777–792.
[65] H.A. Foster, J.M. Bridger, The genome and the nucleus: a marriage made by evolution. Genome organisation and nuclear architecture, Chromosoma 114 (2005) 212–229.
[66] M. Branco, A. Pombo, Chromosome organization: new facts, new models, Trends Cell Biol. 17 (2007) 127–134.
[67] H. Albiez, M. Cremer, C. Tiberi, L. Vecchio, L. Schermelleh, S. Dittrich, K. Küpper, B. Joffe, T. Thormeyer, J. von Hase, S. Yang, K. Rohr, H. Leonhardt, I. Solovei, C. Cremer, S. Fakan, T. Cremer, Chromatin domains and the interchromatin compartment form structurally defined and functionally interacting nuclear networks, Chromosome Res. 14 (2006) 707–733.
[68] D. Marenduzzo, I. Faro-Trindade, P. Cook, What are the molecular ties that maintain genomic loops? Trends Genet. 23 (2007) 126–133.
[69] K. Rippe, Dynamic organization of the cell nucleus, Curr. Opin. Genet. Dev. 17 (2007) 373–380.
[70] N. Dillon, Heterochromatin structure and function, Biol. Cell 96 (2004) 631–637.
[71] S.I. Grewal, S. Jia, Heterochromatin revisited, Nat. Rev. Genet. 8 (2006) 35–46.
[72] L. Guelen, L. Pagie, E. Brasset, W. Meuleman, M.B. Faza, W. Talhout, B.H. Eussen, A. de Klein, L. Wessels, W. de Laat, B. van Steensel, Domain organization of human chromosomes revealed by mapping of nuclear lamina interactions, Nature (2008).
[73] K. Maeshima, M. Eltsov, Packaging the genome: the structure of mitotic chromosomes, J. Biochem. 143 (2008) 145–153.
[74] J.F. Marko, Micromechanical studies of mitotic chromosomes, Chromosome Res. 16 (2008) 469–497.
[75] T. Hirano, Condensins: organizing and segregating the genome, Curr. Biol. 15 (2005) 265–275.
[76] N. Kireeva, M. Lakonishok, I. Kireev, T. Hirano, A. Belmont, Visualization of early chromosome condensation: a hierarchical folding, axial glue model of chromosome structure, J. Cell Biol. 166 (2004) 775–785.
[77] T. Weidemann, M. Wachsmuth, T. Knoch, G. Müller, W. Waldeck, J. Langowski, Counting nucleosomes in living cells with a combination of fluorescence correlation spectroscopy and confocal imaging, J. Mol. Biol. 334 (2003) 229–240.
[78] S. Görisch, M. Wachsmuth, K. Fejes Tóth, P. Lichter, K. Rippe, Histone acetylation increases chromatin accessibility, J. Cell Sci. 118 (2005) 5825–5834.
[79] K. Fejes Tóth, T.A. Knoch, M. Wachsmuth, M. Stöhr, M. Frank-Stöhr, C.P. Bacher, G. Müller, K. Rippe, Trichostatin A induced histone acetylation causes decondensation of interphase chromatin, J. Cell Sci. 117 (2004) 4277–4287.
[80] S.M. Janicki, T. Tsukamoto, S.E. Salghetti, W.P. Tansey, R. Sachidanandam, K.V. Prasanth, T. Ried, Y. Shav-Tal, E. Bertrand, R.H. Singer, D.L. Spector, From silencing to gene expression: real-time analysis in single cells, Cell 116 (2004) 683–698.
[81] P.J. Verschure, I. van der Kraan, E.M. Manders, D. Hoogstraten, A.B. Houtsmuller, R. van Driel, Condensed chromatin domains in the mammalian nucleus are accessible to large macromolecules, EMBO Rep. 4 (2003) 861–866.
[82] C. Pack, K. Saito, M. Tamura, M. Kinjo, Microenvironment and effect of energy depletion in the nucleus analyzed by mobility of multiple oligomeric EGFPs, Biophys. J. 91 (2006) 3921–3936.
[83] S.M. Görisch, K. Richter, M.O. Scheuermann, H. Herrmann, P. Lichter, Diffusion-limited compartmentalization of mammalian cell nuclei assessed by microinjected macromolecules, Exp. Cell Res. 289 (2003) 282–294.
[84] Y. Tseng, J.S. Lee, T.P. Kole, I. Jiang, D. Wirtz, Micro-organization and viscoelasticity of the interphase nucleus revealed by particle nanotracking, J. Cell Sci. 117 (2004) 2159–2167.
[85] S.M. Görisch, M. Wachsmuth, C. Ittrich, C.P. Bacher, K. Rippe, P. Lichter, Nuclear body movement is determined by chromatin accessibility and dynamics, Proc. Natl. Acad. Sci. U.S.A. 101 (2004) 13221–13226.
[86] M. Reichenzeller, A. Burzlaff, P. Lichter, H. Herrmann, In vivo observation of a nuclear channel-like system: evidence for a distinct interchromosomal domain compartment in interphase cells, J. Struct. Biol. 129 (2000) 175–185.
[87] J.M. Bridger, H. Herrmann, C. Münkel, P. Lichter, Identification of an interchromosomal compartment by polymerization of nuclear-targeted vimentin, J. Cell Sci. 111 (Pt 9) (1998) 1241–1253.
[88] M.O. Scheuermann, A.E. Murmann, K. Richter, S.M. Gorisch, H. Herrmann, P. Lichter, Characterization of nuclear compartments identified by ectopic markers in mammalian cells with distinctly different karyotype, Chromosoma 114 (2005) 39–53.
[89] R.M. Zirbel, U.R. Mathieu, A. Kurz, T. Cremer, P. Lichter, Evidence for a nuclear compartment of transcription and splicing located at chromosome domain boundaries, Chromosome Res. 1 (1993) 93–106.
[90] K. Richter, M. Reichenzeller, S.M. Görisch, U. Schmidt, M.O. Scheuermann, H. Herrmann, P. Lichter, Characterization of a nuclear compartment shared by nuclear bodies applying ectopic protein expression and correlative light and electron microscopy, Exp. Cell Res. 303 (2005) 128–137.
[91] K. Richter, M. Nessling, P. Lichter, Experimental evidence for the influence of molecular crowding on nuclear architecture, J. Cell Sci. (2007).
[92] J. Daban, High concentration of DNA in condensed chromatin, Biochem. Cell Biol. 81 (2003) 91–99.
[93] A.W. McDowall, J.M. Smith, J. Dubochet, Cryo-electron microscopy of vitrified chromosomes in situ, EMBO J. 5 (1986) 1395–1402.
[94] D. Chen, M. Dundr, C. Wang, A. Leung, A. Lamond, T. Misteli, S. Huang, Condensed mitotic chromatin is accessible to transcription factors and chromatin structural proteins, J. Cell Biol. 168 (2005) 41–54.
[95] M.J. Saxton, K. Jacobson, Single-particle tracking: applications to membrane dynamics, Annu. Rev. Biophys. Biomol. Struct. 26 (1997) 373–399.
[96] G. Carrero, D. McDonald, E. Crawford, G. de Vries, M.J. Hendzel, Using FRAP and mathematical modeling to determine the in vivo kinetics of nuclear proteins, Methods 29 (2003) 14–28.
[97] B. Sprague, Analysis of binding reactions by fluorescence recovery after photobleaching, Biophys. J. 86 (2004) 3473–3495.
[98] R.D. Phair, P. Scaffidi, C. Elbi, J. Vecerová, A. Dey, K. Ozato, D.T. Brown, G. Hager, M. Bustin, T. Misteli, Global nature of dynamic protein-chromatin interactions in vivo: three-dimensional genome scanning and dynamic interaction networks of chromatin proteins, Mol. Cell. Biol. 24 (2004) 6393–6402.
[99] J.G. McNally, Quantitative FRAP in analysis of molecular binding dynamics in vivo, Methods Cell Biol 85 (2008) 329–351.
[100] P.H. von Hippel, O.G. Berg, Facilitated target location in biological systems, J. Biol. Chem. 264 (1989) 675–678.
[101] S.E. Halford, J.F. Marko, How do site-specific DNA-binding proteins find their targets? Nucleic Acids Res. 32 (2004) 3040–3052.
[102] O.G. Berg, P.H. von Hippel, Diffusion-controlled macromolecular interactions, Annu. Rev. Biophys. Biophys. Chem. 14 (1985) 131–160.
[103] B.W. Pontius, Close encounters: why unstructured, polymeric domains can increase rates of specific macromolecular association, Trends Biochem. Sci. 18 (1993) 181–186.
[104] A. Bunde, S. Havlin (Eds.), Fractals and Disordered Systems, 2nd ed., Springer-Verlag, Berlin, 1995.
[105] M. Wachsmuth, K. Weisshart, Fluorescence photobleaching and fluorescence correlation spectroscopy: two complementary technologies to study molecular dynamics in living cells, in: S.L. Shorte, F. Frischknecht (Eds.), Imaging Cellular and Molecular Biological Functions, Springer Verlag, Heidelberg, 2007.
[106] Y. Sako, A. Kusumi, Compartmentalized structure of the plasma membrane for receptor movements as revealed by a nanometer-level motion analysis, J. Cell Biol. 125 (1994) 1251–1264.
[107] R. Simson, B. Yang, S.E. Moore, P. Doherty, F.S. Walsh, K.A. Jacobson, Structural mosaicism on the submicron scale in the plasma membrane, Biophys. J. 74 (1998) 297–308.
[108] A. Blumen, J. Klafter, B.S. White, G. Zumofen, Continuous-time random walks on fractals, Phys. Rev. Lett. 53 (1984) 1301–1304.
[109] H. Scher, M. Lax, Stochastic transport in a disordered solid. I. Theory, Phys. Rev. B. 7 (1973) 4491–4502.
[110] G. Cabal, A. Genovesio, S. Rodriguez-Navarro, C. Zimmer, O. Gadal, A. Lesne, H. Buc, F. Feuerbach-Fournier, J. Olivo-Marin, E. Hurt, U. Nehrbass, SAGA interacting factors confine sub-diffusion of transcribed genes to the nuclear envelope, Nature 441 (2006) 770–773.
[111] J. Beaudouin, F. Mora-Bermúdez, T. Klee, N. Daigle, J. Ellenberg, Dissecting the contribution of diffusion and interactions to the mobility of nuclear proteins. Biophys. J. 90 (2006) 1878–1894.
[112] H. Merlitz, K.V. Klenin, C.X. Wu, J. Langowski, Facilitated diffusion of DNA-binding proteins: Simulation of large systems, J. Chem. Phys. 125 (2006) 014906.
[113] R. Peters, J. Peters, K.H. Tews, W. Bahr, A microfluorimetric study of translational diffusion in erythrocyte membranes, Biochim. Biophys. Acta 367 (1974) 282–294.
[114] D. Axelrod, D.E. Koppel, J. Schlessinger, E. Elson, W.W. Webb, Mobility measurement by analysis of fluorescence photobleaching recovery kinetics, Biophys. J. 16 (1976) 1055–1069.
[115] D. Magde, E.L. Elson, W.W. Webb, Thermodynamic fluctuations in a reacting system - measurement by fluorescence correlation spectroscopy, Phys. Rev. Lett. 29 (1972) 705–708.
[116] D. Magde, E.L. Elson, W.W. Webb, Fluorescence correlation spectroscopy. II. An experimental realization, Biopolymers 13 (1974) 29–61.
[117] E.L. Elson, D. Magde, Fluorescence correlation spectroscopy. I. Conceptual basis and theory, Biopolymers 13 (1974) 1–27.
[118] H. Qian, M.P. Sheetz, E.L. Elson, Single particle tracking. Analysis of diffusion and flow in two-dimensional systems, Biophys. J. 60 (1991) 910–921.
[119] T. Förster, Zwischenmolekulare Energiewanderung und Fluoreszenz, Ann. Phys. 2 (1948) 55–75.
[120] T. Förster, Fluoreszenz organischer Verbindungen, Vandenhoeck & Ruprecht, Göttingen, 1951.
[121] M. Wachsmuth, W. Waldeck, J. Langowski, Anomalous diffusion of fluorescent probes inside living cell nuclei investigated by spatially-resolved fluorescence correlation spectroscopy, J. Mol. Biol. 298 (2000) 677–689.
[122] J.C. Politz, R.A. Tuft, K.V. Prasanth, N. Baudendistel, K.E. Fogarty, L.M. Lifshitz, J. Langowski, D.L. Spector, T. Pederson, Rapid, diffusional shuttling of poly(A) RNA

between nuclear speckles and the nucleoplasm, Mol. Biol. Cell 17 (2006) 1239–1249.
[123] H. Kimura, P.R. Cook, Kinetics of core histones in living human cells: little exchange of H3 and H4 and some rapid exchange of H2B, J. Cell Biol. 153 (2001) 1341–1353.
[124] T. Misteli, A. Gunjan, R. Hock, M. Bustin, D.T. Brown, Dynamic binding of histone H1 to chromatin in living cells, Nature 408 (2000) 877–881.
[125] M.A. Lever, J.P. Th'ng, X. Sun, M.J. Hendzel, Rapid exchange of histone H1.1 on chromatin in living human cells, Nature 408 (2000) 873–876.
[126] T. Kues, R. Peters, U. Kubitscheck, Visualization and tracking of single protein molecules in the cell nucleus, Biophys. J. 80 (2001) 2954–2967.
[127] A.F. Straight, A.S. Belmont, C.C. Robinett, A.W. Murray, GFP tagging of budding yeast chromosomes reveals that protein-protein interactions can mediate sister chromatid cohesion, Curr. Biol. 6 (1996) 1599–1608.
[128] J. Rino, J.M. Desterro, T.R. Pacheco, T.W. Gadella Jr., M. Carmo-Fonseca, Splicing factors SF1 and U2AF associate in extraspliceosomal complexes, Mol. Cell. Biol. 28 (2008) 3045–3057.
[129] C.P. Bacher, M. Reichenzeller, C. Athale, H. Herrmann, R. Eils, 4-D single particle tracking of synthetic and proteinaceous microspheres reveals preferential movement of nuclear particles along chromatin - poor tracks, BMC Cell Biol. 5 (2004) 45.
[130] B. Rieger, C. Molenaar, R.W. Dirks, L.J. Van Vliet, Alignment of the cell nucleus from labeled proteins only for 4D in vivo imaging, Microsc. Res. Tech. 64 (2004) 142–150.
[131] D.M. Soumpasis, Theoretical analysis of fluorescence photobleaching recovery experiments, Biophys. J. 41 (1983) 95–97.
[132] A. Calapez, H.M. Pereira, A. Calado, J. Braga, J. Rino, C. Carvalho, J.P. Tavanez, E. Wahle, A.C. Rosa, M. Carmo-Fonseca, The intranuclear mobility of messenger RNA binding proteins is ATP dependent and temperature sensitive, J. Cell Biol. 159 (2002) 795–805.
[133] M. Dundr, U. Hoffmann-Rohrer, Q. Hu, I. Grummt, L.I. Rothblum, R.D. Phair, T. Misteli, A kinetic framework for a mammalian RNA polymerase in vivo, Science 298 (2002) 1623–1626.
[134] P. Hinow, The DNA binding activity of p53 displays reaction–diffusion kinetics, Biophys. J. 91 (2006) 330–342.
[135] J. Braga, J.G. McNally, M. Carmo-Fonseca, A reaction–diffusion model to study RNA motion by quantitative fluorescence recovery after photobleaching, Biophys. J. 92 (2007) 2694–2703.
[136] Y. Tardy, J.L. McGrath, J.H. Hartwig, C.F. Dewey, Interpreting photoactivated fluorescence microscopy measurements of steady-state actin dynamics, Biophys. J. 69 (1995) 1674–1682.
[137] J.L. McGrath, Y. Tardy, C.F. Dewey, J.J. Meister, J.H. Hartwig, Simultaneous measurements of actin filament turnover, filament fraction, and monomer diffusion in endothelial cells, Biophys. J. 75 (1998) 2070–2078.
[138] N.B. Cole, C.L. Smith, N. Sciaky, M. Terasaki, M. Edidin, J. Lippincott-Schwartz, Diffusional mobility of Golgi proteins in membranes of living cells, Science 273 (1996) 797–801.
[139] L.S. Cutts, P.A. Roberts, J. Adler, M.C. Davies, C.D. Melia, Determination of localized diffusion coefficients in gels using confocal scanning laser microscopy, J. Microsc. 180 (1995) 131–139.
[140] R. Peters, A. Brünger, K. Schulten, Continuous fluorescence microphotolysis: a sensitive method for study of diffusion processes in single cells, Proc. Natl. Acad. Sci. U.S.A. 78 (1981) 962–966.
[141] M. Wachsmuth, T. Weidemann, G. Muller, U.W. Hoffmann-Rohrer, T.A. Knoch, W. Waldeck, J. Langowski, Analyzing intracellular binding and diffusion with continuous fluorescence photobleaching, Biophys. J. 84 (2003) 3353–3363.
[142] J. Ricka, T. Binkert, Direct measurement of a distinct correlation function by fluorescence cross correlation, Phys. Rev. A. 39 (1989) 2646–2652.
[143] P. Schwille, F.J. Meyer-Almes, R. Rigler, Dual-color fluorescence cross-correlation spectroscopy for multicomponent diffusional analysis in solution, Biophys. J. 72 (1997) 1878–1886.
[144] K. Rippe, Simultaneous binding of two DNA duplexes to the NtrC-enhancer complex studied by two-color fluorescence cross-correlation spectroscopy, Biochemistry 39 (2000) 2131–2139.
[145] R. Strohner, M. Wachsmuth, K. Dachauer, J. Mazurkiewicz, J. Hochstätter, K. Rippe, G. Längst, A 'loop recapture' mechanism for ACF-dependent nucleosome remodeling, Nat. Struct. Mol. Biol. 12 (2005) 683–690.
[146] A. Gennerich, D. Schild, Fluorescence correlation spectroscopy in small cytosolic compartments depends critically on the diffusion model used, Biophys. J. 79 (2000) 3294–3306.
[147] C. Fradin, A. Abu-Arish, R. Granek, M. Elbaum, Fluorescence correlation spectroscopy close to a fluctuating membrane, Biophys. J. 84 (2003) 2005–2020.
[148] N.O. Petersen, P.L. Hoddelius, P.W. Wiseman, O. Seger, K.E. Magnusson, Quantitation of membrane receptor distributions by image correlation spectroscopy: concept and application, Biophys. J. 65 (1993) 1135–1146.
[149] N.O. Petersen, FCS and spatial correlations on biological surfaces, in: R. Rigler, E.S. Elson (Eds.), Fluorescence Correlation Spectroscopy - Theory and Applications, Springer, Heidelberg, 2001, pp. 162–184.
[150] M.A. Digman, P. Sengupta, P.W. Wiseman, C.M. Brown, A.R. Horwitz, E. Gratton, Fluctuation correlation spectroscopy with a laser-scanning microscope: exploiting the hidden time structure, Biophys. J. 88 (2005) L33–36.
[151] A. Hoppe, Quantitative FRET microscopy of live cells, in: S.L. Shorte, F. Frischknecht (Eds.), Imaging Cellular and Molecular Biological Functions, Springer Verlag, Heidelberg, 2007.
[152] E.A. Jares-Erijman, T.M. Jovin, FRET imaging, Nat. Biotechnol. 21 (2003) 1387–1395.
[153] H. Kimura, Histone dynamics in living cells revealed by photobleaching, DNA Repair (Amst) 4 (2005) 939–950.
[154] P. Hemmerich, S. Weidtkamp-Peters, C. Hoischen, L. Schmiedeberg, I. Erliandri, S. Diekmann, Dynamics of inner kinetochore assembly and maintenance in living cells, J. Cell Biol. 180 (2008) 1101–1114.
[155] D. Gerlich, B. Koch, F. Dupeux, J.M. Peters, J. Ellenberg, Live-cell imaging reveals a stable cohesin-chromatin interaction after but not before DNA replication, Curr. Biol. 16 (2006) 1571–1578.
[156] O.I. Kulaeva, D.A. Gaykalova, V.M. Studitsky, Transcription through chromatin by RNA polymerase II: histone displacement and exchange, Mutat. Res. 618 (2007) 116–129.
[157] E. Meshorer, D. Yellajoshula, E. George, P. Scambler, D. Brown, T. Misteli, Hyperdynamic plasticity of chromatin proteins in pluripotent embryonic stem cells, Dev. Cell 10 (2006) 105–116.
[158] E. Meshorer, T. Misteli, Chromatin in pluripotent embryonic stem cells and differentiation, Nat. Rev. Mol. Cell Biol. 7 (2006) 540–546.
[159] J.F. Kepert, J. Mazurkiewicz, G. Heuvelman, K. Fejes Tóth, K. Rippe, NAP1 modulates binding of linker histone H1 to chromatin and induces an extended chromatin fiber conformation, J. Biol. Chem. 280 (2005) 34063–34072.
[160] J. Mazurkiewicz, J. Kepert, K. Rippe, On the mechanism of nucleosome assembly by histone chaperone NAP1, J. Biol. Chem. 281 (2006) 16462–16472.
[161] P. Hajkova, K. Ancelin, T. Waldmann, N. Lacoste, U. Lange, F. Cesari, C. Lee, G. Almouzni, R. Schneider, M. Surani, Chromatin dynamics during epigenetic reprogramming in the mouse germ line, Nature 452 (2008) 877–881.
[162] T. Ito, T. Ikehara, T. Nakagawa, W.L. Kraus, M. Muramatsu, p300-mediated acetylation facilitates the transfer of histone H2A–H2B dimers from nucleosomes to a histone chaperone, Genes Dev. 14 (2000) 1899–1907.
[163] M. Zofall, J. Persinger, S.R. Kassabov, B. Bartholomew, Chromatin remodeling by ISW2 and SWI/SNF requires DNA translocation inside the nucleosome, Nat. Struct. Mol. Biol. 13 (2006) 339–346.
[164] G. Mizuguchi, X. Shen, J. Landry, W.H. Wu, S. Sen, C. Wu, ATP-driven exchange of histone H2AZ variant catalyzed by SWR1 chromatin remodeling complex, Science 303 (2004) 343–348.
[165] T. Cheutin, A.J. McNairn, T. Jenuwein, D.M. Gilbert, P.B. Singh, T. Misteli, Maintenance of stable heterochromatin domains by dynamic HP1 binding, Science 299 (2003) 721–725.
[166] R. Festenstein, S.N. Pagakis, K. Hiragami, D. Lyon, A. Verreault, B. Sekkali, D. Kioussis, Modulation of heterochromatin protein 1 dynamics in primary mammalian cells, Science 299 (2003) 719–721.
[167] J.R. Abney, B. Cutler, M.L. Fillbach, D. Axelrod, B.A. Scalettar, Chromatin dynamics in interphase nuclei and its implications for nuclear structure, J. Cell Biol. 137 (1997) 1459–1468.
[168] D. Zink, T. Cremer, R. Saffrich, R. Fischer, M.F. Trendelenburg, W. Ansorge, E.H. Stelzer, Structure and dynamics of human interphase chromosome territories in vivo, Hum. Genet. 102 (1998) 241–251.
[169] E.M. Manders, H. Kimura, P.R. Cook, Direct imaging of DNA in living cells reveals the dynamics of chromosome formation, J. Cell Biol. 144 (1999) 813–821.
[170] C.C. Robinett, A. Straight, G. Li, C. Willhelm, G. Sudlow, A. Murray, A.S. Belmont, In vivo localization of DNA sequences and visualization of large-scale chromatin organization using lac operator/repressor recognition, J. Cell Biol. 135 (1996) 1685–1700.
[171] C.H. Chuang, A.S. Belmont, Moving chromatin within the interphase nucleus-controlled transitions? Semin Cell Dev Biol 18 (2007) 698–706.
[172] S.M. Görisch, P. Lichter, K. Rippe, Mobility of multi-subunit complexes in the nucleus: chromatin dynamics and accessibility of nuclear subcompartments, Histochem. Cell Biol. 123 (2005) 217–228.
[173] E. Soutoglou, J. Dorn, K. Sengupta, M. Jasin, A. Nussenzweig, T. Ried, G. Danuser, T. Misteli, Positional stability of single double-strand breaks in mammalian cells, Nat. Cell Biol. (2007).
[174] C. Chuang, A. Carpenter, B. Fuchsova, T. Johnson, P. de Lanerolle, A. Belmont, Long-range directional movement of an interphase chromosome site, Curr. Biol. 16 (2006) 825–831.
[175] G.L. Hager, C. Elbi, T.A. Johnson, T. Voss, A.K. Nagaich, R.L. Schiltz, Y. Qiu, S. John, Chromatin dynamics and the evolution of alternate promoter states, Chromosome Res. 14 (2006) 107–116.
[176] H. Kimura, K. Sugaya, P.R. Cook, The transcription cycle of RNA polymerase II in living cells, J. Cell Biol. 159 (2002) 777–782.
[177] X. Darzacq, Y. Shav-Tal, V. de Turris, Y. Brody, S.M. Shenoy, R.D. Phair, R.H. Singer, In vivo dynamics of RNA polymerase II transcription, Nat. Struct. Mol. Biol. (2007).
[178] J. Yao, K.M. Munson, W.W. Webb, J.T. Lis, Dynamics of heat shock factor association with native gene loci in living cells, Nature 442 (2006) 1050–1053.
[179] W. Vermeulen, A.B. Houtsmuller, The transcription cycle in vivo. A blind watchmaker at work, Mol. Cell 10 (2002) 1264–1266.
[180] J. Essers, A.F. Theil, C. Baldeyron, W.A. van Cappellen, A.B. Houtsmuller, R. Kanaar, W. Vermeulen, Nuclear dynamics of PCNA in DNA replication and repair, Mol. Cell. Biol. 25 (2005) 9350–9359.
[181] A. Sporbert, P. Domaing, H. Leonhardt, M.C. Cardoso, PCNA acts as a stationary loading platform for transiently interacting Okazaki fragment maturation proteins, Nucleic Acids Res. 33 (2005) 3521–3528.
[182] A. Sporbert, A. Gahl, R. Ankerhold, H. Leonhardt, M.C. Cardoso, DNA polymerase clamp shows little turnover at established replication sites but sequential de novo assembly at adjacent origin clusters, Mol. Cell 10 (2002) 1355–1365.
[183] A. Houtsmuller, Action of DNA repair endonuclease ERCC1/XPF in living cells, Science 284 (1999) 958–961.
[184] J. Haince, M. Ouellet, D. Mcdonald, M. Hendzel, G. Poirier, Dynamic relocation of poly(ADP-ribose) glycohydrolase isoforms during radiation-induced DNA damage, Biochim. Biophys. Acta 1763 (2006) 226–237.

[185] A. Politi, M. Moné, A. Houtsmuller, D. Hoogstraten, W. Vermeulen, R. Heinrich, R. van Driel, Mathematical modeling of nucleotide excision repair reveals efficiency of sequential assembly strategies, Mol. Cell 19 (2005) 679–690.
[186] M.S. Luijsterburg, J. Goedhart, J. Moser, H. Kool, B. Geverts, A.B. Houtsmuller, L.H. Mullenders, W. Vermeulen, R. van Driel, Dynamic in vivo interaction of DDB2 E3 ubiquitin ligase with UV-damaged DNA is independent of damage-recognition protein XPC, J. Cell Sci. 120 (2007) 2706–2716.
[187] J. Essers, W. Vermeulen, A.B. Houtsmuller, DNA damage repair: anytime, anywhere? Curr. Opin. Cell Biol. 18 (2006) 240–246.
[188] D. Hoogstraten, A.L. Nigg, H. Heath, L.H. Mullenders, R. van Driel, J.H. Hoeijmakers, W. Vermeulen, A.B. Houtsmuller, Rapid switching of TFIIH between RNA polymerase I and II transcription and DNA repair in vivo, Mol. Cell 10 (2002) 1163–1174.
[189] M.S. Jurica, M.J. Moore, Pre-mRNA splicing: awash in a sea of proteins, Mol. Cell 12 (2003) 5–14.
[190] H. Le Hir, M.J. Moore, L.E. Maquat, Pre-mRNA splicing alters mRNP composition: evidence for stable association of proteins at exon–exon junctions, Genes Dev. 14 (2000) 1098–1108.
[191] S. Bessonov, M. Anokhina, C.L. Will, H. Urlaub, R. Luhrmann, Isolation of an active step I spliceosome and composition of its RNP core, Nature 452 (2008) 846–850.
[192] T.O. Tange, T. Shibuya, M.S. Jurica, M.J. Moore, Biochemical analysis of the EJC reveals two new factors and a stable tetrameric protein core, RNA 11 (2005) 1869–1883.
[193] Z. Zhang, A.R. Krainer, Splicing remodels messenger ribonucleoprotein architecture via eIF4A3-dependent and -independent recruitment of exon junction complex components, Proc. Natl. Acad. Sci. U.S.A. 104 (2007) 11574–11579.
[194] M.J. Kruhlak, M.A. Lever, W. Fischle, E. Verdin, D.P. Bazett-Jones, M.J. Hendzel, Reduced mobility of the alternate splicing factor (ASF) through the nucleoplasm and steady state speckle compartments, J. Cell Biol. 150 (2000) 41–51.
[195] R.D. Phair, T. Misteli, High mobility of proteins in the mammalian cell nucleus, Nature 404 (2000) 604–609.
[196] J. Rino, T. Carvalho, J. Braga, J.M. Desterro, R. Luhrmann, M. Carmo-Fonseca, A stochastic view of spliceosome assembly and recycling in the nucleus, PLoS Comput Biol 3 (2007) 2019–2031.
[197] Y. Ishihama, H. Tadakuma, T. Tani, T. Funatsu, The dynamics of pre-mRNAs and poly(A)+ RNA at speckles in living cells revealed by iFRAP studies, Exp. Cell. Res. 314 (2008) 748–762.
[198] U. Schmidt, K. Richter, A.B. Berger, P. Lichter, In vivo BiFC analysis of Y14 and NXF1 mRNA export complexes: preferential localization within and around SC35 domains, J. Cell Biol. 172 (2006) 373–381.
[199] C. Molenaar, A. Abdulle, A. Gena, H.J. Tanke, R.W. Dirks, Poly(A)+ RNAs roam the cell nucleus and pass through speckle domains in transcriptionally active and inactive cells, J. Cell Biol. 165 (2004) 191–202.
[200] F. Boisvert, S. van Koningsbruggen, J. Navascués, A. Lamond, The multifunctional nucleolus, Nat. Rev. Mol. Cell. Biol. (2007).
[201] K.E. Handwerger, C. Murphy, J.G. Gall, Steady-state dynamics of Cajal body components in the Xenopus germinal vesicle, J. Cell Biol. 160 (2003) 495–504.
[202] S. Weidtkamp-Peters, T. Lenser, D. Negorev, N. Gerstner, T.G. Hofmann, G. Schwanitz, C. Hoischen, G. Maul, P. Dittrich, P. Hemmerich, Dynamics of component exchange at PML nuclear bodies, J. Cell Sci. 121 (2008) 2731–2743.
[203] J.R. Chubb, S. Boyle, P. Perry, W.A. Bickmore, Chromatin motion is constrained by association with nuclear compartments in human cells, Curr. Biol. 12 (2002) 439–445.
[204] C. Molenaar, K. Wiesmeijer, N.P. Verwoerd, S. Khazen, R. Eils, H.J. Tanke, R.W. Dirks, Visualizing telomere dynamics in living mammalian cells using PNA probes, EMBO J. 22 (2003) 6631–6641.
[205] J. Vazquez, A.S. Belmont, J.W. Sedat, Multiple regimes of constrained chromosome motion are regulated in the interphase Drosophila nucleus, Curr. Biol. 11 (2001) 1227–1239.
[206] W.F. Marshall, A. Straight, J.F. Marko, J. Swedlow, A. Dernburg, A. Belmont, A.W. Murray, D.A. Agard, J.W. Sedat, Interphase chromosomes undergo constrained diffusional motion in living cells, Curr. Biol. 7 (1997) 930–939.
[207] V. Levi, Q. Ruan, M. Plutz, A. Belmont, E. Gratton, Chromatin dynamics in interphase cells revealed by tracking in a two-photon excitation microscope, Biophys. J. 89 (2005) 4275–4285.
[208] M.R. Frey, A.G. Matera, Coiled bodies contain U7 small nuclear RNA and associate with specific DNA sequences in interphase human cells, Proc. Natl. Acad. Sci. U.S.A. 92 (1995) 5915–5919.
[209] W. Schul, R. van Driel, L. de Jong, Coiled bodies and U2 snRNA genes adjacent to coiled bodies are enriched in factors required for snRNA transcription, Mol. Biol. Cell 9 (1998) 1025–1036.
[210] E.Y. Jacobs, M.R. Frey, W. Wu, T.C. Ingledue, T.C. Gebuhr, L. Gao, W.F. Marzluff, A.G. Matera (Eds.), Coiled bodies preferentially associate with U4, U11, and U12 small nuclear RNA genes in interphase HeLa cells but not with U6 and U7 genes, 1999.
[211] J.G. Gall, E.C. Stephenson, H.P. Erba, M.O. Diaz, G. Barsacchi-Pilone, Histone genes are located at the sphere loci of newt lampbrush chromosomes, Chromosoma 84 (1981) 159–171.
[212] H.G. Callan, J.G. Gall, C. Murphy, Histone genes are located at the sphere loci of Xenopus lampbrush chromosomes, Chromosoma 101 (1991) 245–251.
[213] C. Shiels, S.A. Islam, R. Vatcheva, P. Sasieni, M.J. Sternberg, P.S. Freemont, D. Sheer, PML bodies associate specifically with the MHC gene cluster in interphase nuclei, J. Cell Sci. 114 (2001) 3705–3716.
[214] J. Wang, C. Shiels, P. Sasieni, P.J. Wu, S.A. Islam, P.S. Freemont, D. Sheer, Promyelocytic leukemia nuclear bodies associate with transcriptionally active genomic regions, J. Cell Biol. 164 (2004) 515–526.
[215] T.R. Yeager, A.A. Neumann, A. Englezou, L.I. Huschtscha, J.R. Noble, R.R. Reddel, Telomerase-negative immortalized human cells contain a novel type of promyelocytic leukemia (PML) body, Cancer Res. 59 (1999) 4175–4179.
[216] T. Misteli, J.F. Caceres, D.L. Spector, The dynamics of a pre-mRNA splicing factor in living cells, Nature 387 (1997) 523–527.
[217] P. Bubulya, "On the move"ments of nuclear components in living cells, Exp. Cell Res. 296 (2004) 4–11.
[218] A. Belmont, Dynamics of chromatin, proteins, and bodies within the cell nucleus, Curr. Opin. Cell Biol. 15 (2003) 304–310.
[219] G.L. Hager, C. Elbi, M. Becker, Protein dynamics in the nuclear compartment, Curr. Opin. Genet. Dev. 12 (2002) 137–141.
[220] T. Misteli, The concept of self-organization in cellular architecture, J. Cell Biol. 155 (2001) 181–185.
[221] P.R. Cook, Predicting three-dimensional genome structure from transcriptional activity, Nat. Genet. 32 (2002) 347–352.
[222] A. Kentsis, K.L. Borden, Physical mechanisms and biological significance of supramolecular protein self-assembly, Curr. Protein Pept. Sci. 5 (2004) 125–134.
[223] E. Karsenti, Self-organization in cell biology: a brief history, Nat. Rev. Mol. Cell. Biol. 9 (2008) 255–262.
[224] G. Dellaire, D.P. Bazett-Jones, PML nuclear bodies: dynamic sensors of DNA damage and cellular stress, Bioessays 26 (2004) 963–977.
[225] R.D. Everett, J. Murray, ND10 components relocate to sites associated with herpes simplex virus type 1 nucleoprotein complexes during virus infection, J. Virol. 79 (2005) 5078–5089.
[226] K. Yankulov, I. Todorov, P. Romanowski, D. Licatalosi, K. Cilli, S. McCracken, R. Laskey, D.L. Bentley, MCM proteins are associated with RNA polymerase II holoenzyme, Mol. Cell. Biol. 19 (1999) 6154–6163.
[227] C.L. Smith, R. Horowitz-Scherer, J.F. Flanagan, C.L. Woodcock, C.L. Peterson, Structural analysis of the yeast SWI/SNF chromatin remodeling complex, Nat. Struct. Biol. 10 (2003) 141–145.
[228] G. Ficz, R. Heintzmann, D.J. Arndt-Jovin, Polycomb group protein complexes exchange rapidly in living Drosophila, Development 132 (2005) 3963–3976.
[229] X. Ren, C. Vincenz, T.K. Kerppola, Changes in the distributions and dynamics of polycomb repressive complexes during embryonic stem cell differentiation, Mol. Cell. Biol. 28 (2008) 2884–2895.
[230] R.D. Kornberg, The molecular basis of eucaryotic transcription, Cell death and differentiation 14 (2007) 1989–1997.
[231] P. Cramer, RNA polymerase II structure: from core to functional complexes, Curr. Opin. Genet. Dev. 14 (2004) 218–226.
[232] T.I. Lee, R.A. Young, Transcription of eukaryotic protein-coding genes, Annu. Rev. Genet. 34 (2000) 77–137.
[233] D.K. Pokholok, N.M. Hannett, R.A. Young, Exchange of RNA polymerase II initiation and elongation factors during gene expression in vivo, Mol. Cell 9 (2002) 799–809.
[234] C. Maison, G. Almouzni, HP1 and the dynamics of heterochromatin maintenance, Nat. Rev. Mol. Cell. Biol. 5 (2004) 296–304.
[235] O. Seksek, J. Biwersi, A.S. Verkman, Translational diffusion of macromolecule-sized solutes in cytoplasm and nucleus, J. Cell Biol. 138 (1997) 131–142.
[236] R.Y. Tsien, The green fluorescent protein, Annu. Rev. Biochem. 67 (1998) 509–544.
[237] B.R. Terry, E.K. Matthews, J. Haseloff, Molecular characterisation of recombinant green fluorescent protein by fluorescence correlation microscopy, Biochemical and biophysical research communications 217 (1995) 21–27.
[238] D.T. Brown, T. Izard, T. Misteli, Mapping the interaction surface of linker histone H1(0) with the nucleosome of native chromatin in vivo, Nat. Struct. Mol. Biol. 13 (2006) 250–255.
[239] L. Schmiedeberg, K. Weisshart, S. Diekmann, G. Meyer Zu Hoerste, P. Hemmerich, High- and low-mobility populations of HP1 in heterochromatin of mammalian cells, Mol. Biol. Cell 15 (2004) 2819–2833.
[240] I.M. Krouwels, K. Wiesmeijer, T.E. Abraham, C. Molenaar, N.P. Verwoerd, H.J. Tanke, R.W. Dirks, A glue for heterochromatin maintenance: stable SUV39H1 binding to heterochromatin is reinforced by the SET domain, J . Cell Biol. 170 (2005) 537–549.
[241] G.K. Dialynas, S. Terjung, J.P. Brown, R.L. Aucott, B. Baron-Luhr, P.B. Singh, S.D. Georgatos, Plasticity of HP1 proteins in mammalian cells, J. Cell Sci. 120 (2007) 3415–3424.
[242] H. Bornfleth, P. Edelmann, D. Zink, T. Cremer, C. Cremer, Quantitative motion analysis of subchromosomal foci in living cells using four-dimensional microscopy, Biophys. J. 77 (1999) 2871–2886.